Table of Contents

Section 1. Full Synthetic Procedures of ZIF-1 to ZIF-12

General Synthetic Procedures: Benzimidazole, 2-methylimidazole, Indium nitrate pentahydrate and cobalt nitrate hexahydrate were purchased from the Aldrich Chemical Co. and imidazole, *N,N*-dimethylformamaide (DMF), *N*-methylpyrrolidinone (NMP) were purchased from the Fisher Scientific International Inc. *N,N*-diethylformamide (DEF) was obtained from BASF Corperation. Zinc nitrate tetrahydrate was purchased from the EM Science. All starting materials were used without further purifications. All experimental operations were performed in air.

Thus far, ZIF-2, -3, -6, -10 and -12 were only produced at quantities sufficient for single crystal X-ray structure determination because of the microscopic reaction type (ZIF-2 and -6) or impure product (ZIF-3, -10 and -12). The remaining ZIFs were prepared at quantities that allowed bulk characterizations (elemental analysis, infrared spectroscopy and powder X-ray diffraction). In particular, ZIF-8 and -11 were scaled up to gram quantities for a detailed investigation of their porosity, thermal stability and chemical stability.

In this section, we report detailed synthetic procedures for ZIF-1, -3, -4, -7, -8, -9, -10, -11, -12, which are based on the same type of solvothermal reactions in varying size of glass vials, followed by the ones for ZIF-2 and -6, which were discovered by

combinatorial method utilizing the same solvent system and 96-well micro-plates. The synthesis of ZIF-5 is based on a slightly different solvent system and sealed Parr reaction vessels, and is reported at the end of this section.

(ZIF-1 crb) : $Zn(IM)_2{\cdot}(Me_2NH)$. A solid mixture of zinc nitrate tetrahydrate $Zn(NO_3)_2{\cdot}4H_2O$ (0.09 g, 3.44×10^{-4} mol) and imidazole (H-IM) (0.15 g, 2.20×10^{-3} mol) was dissolved in 18 mL DMF in a 20-mL vial. The vial was capped and heated for 24 h in a 85 ºC isothermal oven. The vial was then removed from the oven and allowed to cool to room temperature naturally. Colorless cubic crystals of ZIF-1 thus produced were washed with DMF (3 mL × 3) and dried in air (10 min) (yield: 0.014 g, 17% based on zinc nitrate tetrahydrate).

Elemental analysis $C_8H_{13}N_5Zn = Zn(IM)_2{\cdot}(Me_2NH)$: Calcd. C, 39.28; H, 5.36; N, 28.65. Found C, 39.47; H, 4.39; N, 27.13.

FT-IR **:** (KBr 4000-400cm^{-1}): 3445(br), 3103(w), 2935(w), 2385(w), 2355(w), 1647(s), 1499(m), 1418(w), 1403(w), 1321(w), 1291(w), 1245(w), 1184(w), 1087(s), 1026(w), 985(w), 960(m), 837(w), 761(m), 680(m), 603(w).

(ZIF-3 dft) : $Zn(IM)_2$. A solid mixture of zinc nitrate tetrahydrate $Zn(NO_3)_2{\cdot}4H_2O$

(0.010 g, 3.82×10^{-5} mol) and imidazole (H-IM) (0.030 g, 4.41×10^{-4} mol) was added in a 4-mL vial and dissolved in a mixed solvent of DMF (2 mL) and NMP (1 mL). The vial was capped and heated for 4 d in a 85 ºC isothermal oven. The vial was then removed from the oven and allowed to cool to room temperature naturally. Several prism-shaped crystals formed at the bottom of the vial along with some white powder-like precipitate. The crystals of ZIF-3 were collected manually for single crystal X-ray structure determination.

(ZIF-4 cag) : **$Zn(IM)_2{\cdot}(DMF)(H_2O)$** A solid mixture of zinc nitrate tetrahydrate $Zn(NO_3)_2{\cdot}4H_2O$ (0.040 g, 1.53×10^{-4} mol) and imidazole (H-IM) (0.030 g, 4.41×10^{-4} mol) was dissolved in 3 mL DMF in a 4-mL vial. The vial was capped and heated at a rate 5 ºC /min to 130 ºC in a programmable oven, held at this temperature for 48 h, then cooled at a rate of 0.4 ºC/min to room temperature. Colorless rhombohedral crystals of ZIF-4 thus produced were washed with DMF (3 mL × 3) and dried in the air (10 min) (yield: 0.021 g, 47% based on zinc nitrate tetrahydrate).

Elemental analysis : $C_9H_{15}N_5O_2Zn$ = $Zn(IM)_2{\cdot}(DMF)(H_2O)$: Calcd. C, 37.19; H, 5.20; N, 24.10. Found C, 38.02; H, 4.14; N, 26.74.

FT-IR **:** (KBr 4000-400cm^{-1}): 3427(br), 3111(w), 2926(w), 2856(w), 1688(m),

1612(br), 1502(m), 1392(w), 1282(w), 1247(w), 1176(w), 1091(s), 986(w), 961(m), 846(w), 770(m), 680(m), 490(br).

(ZIF-7 sod) : $Zn(PhIM)_2 \cdot (H_2O)_3$. A solid mixture of zinc nitrate tetrahydrate $Zn(NO_3)_2 \cdot 4H_2O$ (0.030 g, 1.15×10^{-4} mol) and benzimidazole (H-PhIM) (0.010 g, 8.46×10^{-5} mol) was dissolved in 3 mL DMF in a 4-mL vial. The vial was capped and heated at a rate of 5 ºC /min to 130 ºC in a programmable oven, held at this temperature for 48 h, then cooled at a rate of 0.4 ºC/min to room temperature. After removal of mother liquor from the mixture, chloroform (3 mL) was added to the vial. Colorless cubic crystals of ZIF-7 were collected from the upper layer, washed with DMF (3 mL × 3) and dried in air (10 min) (yield: 0.015 g, 37% based on H-PhIM).

Elemental analysis $C_{14}H_{16}N_4O_3Zn = Zn(IM)_2 \cdot (H_2O)_3$: Calcd. C, 47.54; H, 4.56; N, 15.84. Found. C, 46.95; H, 3.57; N, 16.40.

FT-IR : (KBr 4000-400cm^{-1}): 3450(br), 3063(w), 2930(w), 1678(s), 1622(w), 1479(s), 1387(m), 1306(m), 1286(m), 1245(s), 1209(w), 1189(m), 1123(m), 1097(m), 1011(m), 914(m), 781(m), 746(s), 654(m), 476(m), 435(m).

(ZIF-8 sod) : $Zn(MeIM)_2 \cdot (DMF) \cdot (H_2O)_3$. A solid mixture of zinc nitrate tetrahydrate

$Zn(NO_3)_2 \cdot 4H_2O$ (0.210 g, 8.03×10^{-4} mol) and 2-methylimidazole (H-MeIM) (0.060 g, 7.31×10^{-4} mol) was dissolved in 18 mL DMF in a 20-mL vial. The vial was capped and heated at a rate of 5 ºC /min to 140 ºC in a programmable oven, held at this temperature for 24 h, then cooled at a rate of 0.4 ºC/min to room temperature. After removal of mother liquor from the mixture, chloroform (20 mL) was added to the vial. Colorless polyhedral crystals of the product were collected from the upper layer, washed with DMF (10 mL × 3) and dried in air (10 min) (yield: 0.032 g, 25% based on H-MeIM).

Elemental analysis. $C_{11}H_{23}N_5O_4Zn$ = $Zn(MeIM)_2 \cdot (DMF) \cdot (H_2O)_3$ Calcd. C, 37.25; H, 6.54; N, 19.74. Found. C, 37.69; H, 5.22; N, 19.58

FT-IR : (KBr 4000-400cm^{-1}): 3460(w), 3134(w), 2930(m), 2854(w), 2767(w), 2487(w), 2457(w), 1693(s), 1591(w), 1459(s), 1428(s), 1392(m), 1311(s), 1265(w), 1189(m), 1148(s), 1091(m), 1000(m), 960(w), 766(s), 695(m), 664(m), 425(s).

(ZIF-9 sod) : $Co(PhIM)_2 \cdot (DMF)(H_2O)$. A solid mixture of cobalt nitrate hexahydrate $Co(NO_3)_2 \cdot 6H_2O$ (0.210 g, 7.21×10^{-4} mol) and benzimidazole (H-PhIM) (0.060 g, 5.08×10^{-4} mol) was dissolved in 18 mL DMF in a 20-mL vial. The vial was capped and heated at a rate of 5 ºC /min to 130 ºC in a programmable oven, held at this temperature for 48 h, then cooled at a rate of 0.4 ºC/min to room temperature. Purple cubic crystals

thus produced were washed with DMF (3 mL × 3) and dried in air (10 min) (yield: 0.030 g, 30% based on H-PhIM)

Elemental analysis $C_{17}H_{19}N_5O_2Co$ = $Co(PhIM)_2 \cdot (DMF)(H_2O)$ Calcd. C, 53.13; H, 4.98; N,18.22. Found. C, 52.82; H, 4.25; N, 18.23.

FT-IR : (KBr 4000-400cm^{-1}): 3442(br), 3071(w), 2926(w), 1678(s), 1612(w), 1467(s), 1387(w), 1302(w), 1287(m), 1242(s), 1206(w), 1186(w), 1126(w), 1096(w), 1011(w), 916(w), 780(w), 750(s), 660(w), 600(br), 560(w), 475(w).

(ZIF-10 mer) : $Zn(IM)_2$. A solid mixture of zinc nitrate tetrahydrate $Zn(NO_3)_2 \cdot 4H_2O$ (0.010 g, 3.82 × 10^{-5} mol) and imidazole (H-IM) (0.030 g, 4.41 × 10^{-4} mol) was dissolved in 3 mL DMF in a 4-mL vial. The vial was capped and heated for 4 d in an isothermal oven at 85 ºC. The reaction mixture was then allowed to cool to room temperature naturally. Several block-shape crystals of ZIF-10 formed on the wall and bottom, and were separated by hand and collected for single crystal X-ray structure determination.

(ZIF-11 rho) $Zn(PhIM)_2 \cdot (DEF)_{0.9}$. A solid mixture of zinc nitrate tetrahydrate $Zn(NO_3)_2 \cdot 4H_2O$ (0.60 g, 2.3 × 10^{-3} mol) and benzimidazole (H-PhIM) (4.2 g, 3.5 × 10^{-2}

mol) was dissolved in 360 mL DEF in a 500-mL wide-mouth glass jar. The capped jar was heated for 4 d in an isothermal oven at 100 ºC. The jar was then removed from the oven, and allowed to cool to room temperature naturally. Cubic colorless crystals formed on the walls of the jar along with a crystalline powder at the bottom. Although the powder and crystals were proven to be the same phase by powder X-ray diffraction, only the crystals on the wall were used for bulk characterizations. The powder and mother liquor was removed by repeating the cycle of decanting, washing with DMF and sonicating several times. Colorless crystals of ZIF-11 were collected by filtration, washed with DMF (200 mL × 2) and dried in the air (30 min) (yield: 0.21 g, 23% based on $Zn(NO_3)_2{\cdot}4H_2O$).

Elemental analysis $C_{18}H_{21}N_5O_1Zn_1$ = $Zn(PhIM)_2{\cdot}(DEF)_{0.9}$ Calcd. C, 56.94; H, 5.10; N, 17.59. Found: C, 55.69; H, 4.64; N, 17.58.

FT-IR (KBr, 4000~400cm^{-1}) : 3452(br), 3091(w), 3056(w), 2981(w), 2941(w), 2876(w), 2781(w), 2525(w), 1939(w), 1903(w), 1783(w), 1668(s), 1618(m), 1467(s), 1397(w), 1367(w), 1307(m), 1282(m), 1247(m), 1212(w), 1187(m), 1121(m), 1001(m), 911(m), 826(w), 771(m), 751(s), 645(m), 553(m), 520(w), 475(m).

(ZIF-12 rho) : $Co(PhIM)_2$. A solid mixture of cobalt nitrate hexahydrate

$Co(NO_3)_2 \cdot 6H_2O$ (0.010 g, 3.44×10^{-5} mol) and benzimidazole (H-PhIM) (0.030 g, 2.54×10^{-4} mol) was dissolved in 3 mL DEF in a 4-mL vial. The capped vial was heated for 2 d in an isothermal oven at 130 ºC. The reaction mixture was then allowed to cool to room temperature naturally. Several cubic crystals of ZIF-12 formed at the bottom and on the wall of the vial, and they were collected for single crystal X-ray structure determination.

ZIF-2 and ZIF-6 were discovered by combinatorial experimentation utilizing a 96-well glass plate (Zinsser, maximum 0.300 mL reaction mixture per well) as reaction vessel. A 0.150 M solution of imidazole in DMF and a 0.075M solution of $Zn(NO_3)_2 \cdot 4H_2O$ in DMF were used as stock solutions. After the 96-well glass plate was loaded with mixtures of stock solutions dispensed by a programmed liquid handler (Gilson, model 215), it was covered with a PTFE sheet, sealed by fastening the sheet with a metal clamp, then heated in a 85 ºC isothermal oven for 3 days. After reaction, the products were examined under an optical microscope and characterized by single-crystal X-ray diffraction.

(ZIF-2 crb): **$Zn(IM)_2$**. 0.265 mL imidazole stock solution (0.150 M, 3.98×10^{-5} mol) and 0.035 mL $Zn(NO_3)_2 \cdot 4H_2O$ stock solution (0.075 M, 2.63×10^{-6} mol). The product was in the form of small rod-shaped single crystals.

(ZIF-6 gis): **$Zn(IM)_2$**. 0.257 mL imidazole stock solution (0.150 M, 3.86×10^{-5} mol) and 0.043 mL $Zn(NO_3)_2 \cdot 4H_2O$ stock solution (0.075 M, 3.23×10^{-6} mol). The product was in the form of large inter-grown blocks, which could be cut into small single crystals under an optical microscope.

(ZIF-5 gar) : $In_2Zn_3(IM)_{12}$ Indium nitrate pentahydrate, $In(NO_3)_3 \cdot 5H_2O$ (0.156 g, 4.0 × 10^{-4} mol), zinc nitrate tetrahydrate $Zn(NO_3)_2 \cdot 4H_2O$ (0.026 g, 1.0 × 10^{-4} mmol) and imidazole (H-IM) (0.136 g, 2 × 10^{-3} mol) were dissolved in a mixed solvent of DEF/n-butanol (4 mL/2 mL,). After the addition of tetraethylammonium hydroxide (0.05 mL, 35% aqueous solution), the mixture was transferred into a Teflon-lined Parr stainless steel vessel (23 mL) and heated at 150 ºC for 72 hours under autogenous pressure. Pale-yellow crystals thus produced were washed with ethanol and dried in air (yield: 70%, based on zinc nitrate tetrahydrate).

Elemental analysis : $C_{36}H_{36}N_{24}Zn_3In_2 = In_2Zn_3(IM)_{12}$: CHN result, Calcd. C, 35.14; H, 2.95; N, 27.32. Found C, 33.97; H, 2.82; N, 26.22. ICP result, Calcd. Zn, 15.94; In, 18.66. Found Zn, 16.06; In, 18.60.*

FT-IR (KBr 4000-400 cm^{-1}): 3433 (br), 3132 (m), 3112 (m), 2601 (w), 2524 (w), 1697 (m), 1605 (m).†

* ZIF-5 was formulated as $In_2Zn_3(IM)_{12}$ based on single crystal X-ray structure. We found the high In/Zn ratio employed in the synthesis important for the formation of ZIF-5. However, high Indium content also resulted in a small amount of amorphous In-rich impurities (indium oxide or indium hydroxide) as evidenced by the electron microprobe

analysis (EMPA) result of the “bright spots” on crystal surfaces. The content of such impurities was calculated to be 3.3%-4.4% based on the CHN result of the bulk product. However, the Zn and In weight percentage values obtained by ICP analysis of a small number of the clearest crystals manually separated from the bulk product fit the proposed formula well.

† Only the peaks in the wavenumber range important for verifying the deprotonation of imidazole link were labeled. See Figure S1 for details of the spectra.

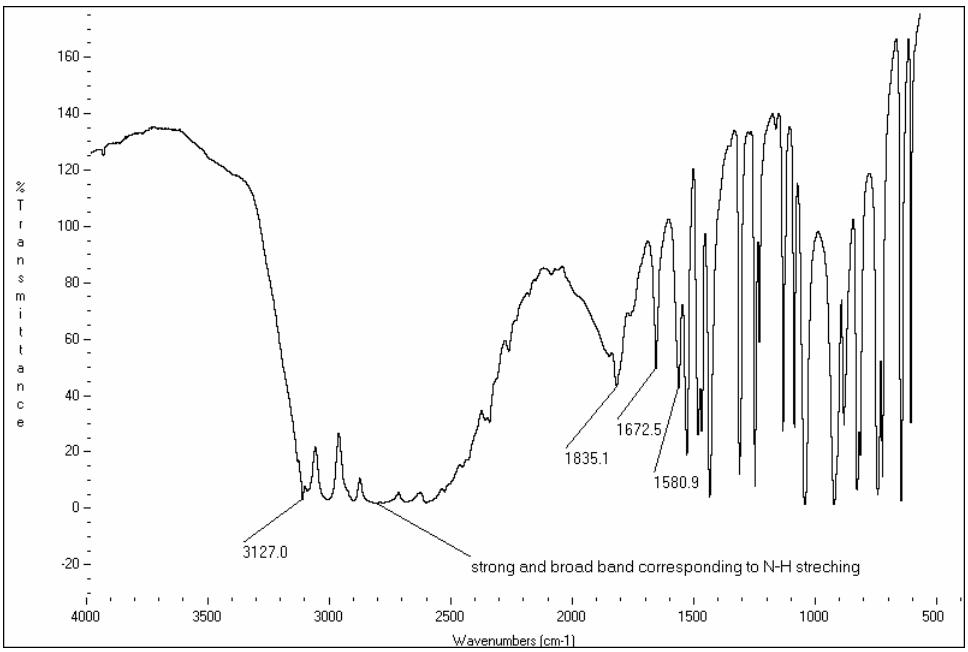

(a)

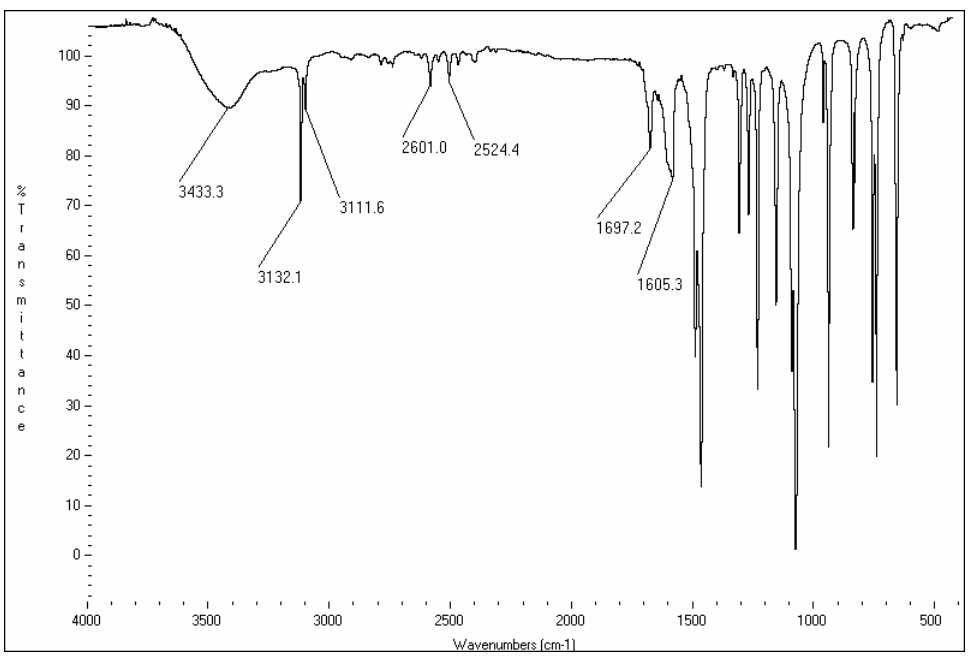

(b)

Figure S1. The FT-IR spectra of (a) imidazole and (b) ZIF-5 (**gar**), $In_2Zn_3(IM)_{12}$.

As shown in Figure S1(a), the FT-IR spectrum of imidazole shows many characteristics of nitrogen-containing heterocycle (see The Aldrich Library of FT-IR spectra, ed II, vol. 3). For pyrazoles, imidazoles, triazoles and tetrazoles, the C-H stretch absorbs near 3125 cm^{-1}. The double bonds on the ring absorb with several bands between 1665-1430 cm^{-1} when the ring system is not substituted so as to allow the formation of tautomers. The NH group absorbs strongly between 3335-2500 cm^{-1}, and in many cases is very similar in shape to the OH stretch of the carboxylic acid dimmer. In the imidazoles, this band is accompanied by a weak band near 1820 cm^{-1}.

As shown in Figure S1(b), the complete disappearance of the strong and broad NH band between 3350-2500 cm^{-1} and the associated weak band near 1820 cm^{-1} indicates that the imidazole links in ZIF-5 $In_2Zn_3(IM)_{12}$ has been fully deprotonated.

Section S2. X-ray Crystallography of ZIF-1 to ZIF-12

General procedures for single crystal data collection, structure solution, and refinement are presented here. Unique details for each structure including treatment of twinning and structural disorders are described prior to the experimental and metrical listings for each structure.

General Data Collection and Refinement Procedures:

Data was collected on a Bruker SMART APEX three circle diffractometer equipped with a CCD area detector and operated at 1800 W power (45 kV, 40 mA) to generate (graphite monochromated) Mo Kα radiation (λ = 0.71073 Å). All crystals were mounted in flame sealed capillaries containing a small amount of mother liquor to prevent desolvation during data collection. Initial ω-ϕ scans of each specimen were taken to gain preliminary unit cell parameters and to assess the moasicity (i.e. breadth of spots between frames) of the crystal to select the required frame width for data collection. For all cases frame widths of 0.3º were judged to be appropriate and full hemispheres of data were collected using the *Bruker SMART*[1] software suite to carry out overlapping ϕ and ω scans. Following data collection, reflections were sampled from all regions of the Ewald sphere to redetermine unit cell parameters for data integration and to check for rotational twinning using *CELL_NOW*.[2] No evidence for crystal decay was

ever encountered. Following exhaustive review of collected frames the resolution of the dataset was judged, and if necessary regions of the frames where no coherent scattering was observed were removed from consideration for data integration using the *Bruker SAINTplus*[3] program. Data was integrated using a narrow frame algorithm (except for ZIF-9 (Co-sod)).[3] Absorption corrections were ineffectual for improving the quality of data, which is not unexpected for small crystals of low density solids containing primarily light atoms. Space group determination and tests for merohedral twinning were carried out using *XPREP*.[3] In all cases the highest possible space group was chosen and no indications of merohedral twinning observed.

All structures were solved by direct methods and refined using the *SHELXTL '97*[4] software suite. Atoms were located from iterative examination of difference F-maps following least squares refinements of the earlier models. Final models were refined anisotropically until full convergence was achieved with all shifts being zero. However, several structures contained disordered components of the ZIF frameworks. In these cases disordered groups were refined isotropically as independent free variables. Hydrogen atoms were placed in calculated positions (C—H = 0.97 Å) and included as riding atoms with isotropic displacement parameters 1.2–1.5 times U_{eq} of the attached C atoms. Modeling of electron density within the voids of the frameworks

did not lead to identification of guest entities in all structures due to the lowered resolution of the data. This challenge, which is typical of porous crystals that contain solvent filled pores, lies in the raw data where observed strong (high intensity) scattering becomes limited to 1.0 Å, with higher resolution data present but weak (low intensity). As is a common strategy for improving X-ray data, increasing the exposure time of the crystal to X-rays did not ameliorate the quality of the high angle data in these cases, as the intensity from low angle data saturated the detector and minimal improvement in the high angle data was achieved. Additionally, diffuse scattering from the highly disordered solvent in the void spaces within the crystal and from the capillary used mount the crystal contributes to the background noise and the 'washing out' of high angle data. The only optimal crystals suitable for analysis were generally small and weakly diffracting, and unfortunately, larger crystals, which might improve the quality of the data, presented a lowered degree of crystallinity and optimization of crystal growing conditions for large high-quality specimens has not yet been fruitful. For almost all structures it was also more reasonable to model against data collected at elevated temperatures (-50 to -15 °C, rather than -120 to -100 °C) when guest entities in the structures where allowed to move freely and therefore did not contribute coherent scattering terms to the observed structure factors. Conversely, at cryogenic temperatures

it was found that free solvent in the crystal will 'freeze' into non-ordered arrays within the pore structure. In such cases the modeling of the disordered guest entities becomes intractable and interferes with determination of the ZIF framework. Thus, electron density within void spaces which could not be assigned to any definite guest entity was modeled as isolated oxygen atoms, and the foremost errors in all the models lies with assignment of guest electron density. Nonetheless, assignment and refinement of the metal-organic ZIF framework atoms was unambiguous, as judged by the resulting bond and angle metrics which are chemically accurate and precise values. All structures were examined using the *Adsym* subroutine of PLATON[5] to assure that no additional symmetry could be applied to the models. All ellipsoids in ORTEP diagrams are displayed at the 30 % probability level unless noted otherwise.

1. Bruker (1998). *SMART*. Version 5.053. Bruker AXS Inc., Madison,Wisconsin, USA.
2. Sheldrick, G. M. (2004). *CELL_NOW*. University of Göttingen, Germany. Steiner, Th. (1998). *Acta Cryst*. B54, 456–463.
3. Bruker (2004). *SAINT-Plus* (Version 7.03). Bruker AXS Inc., Madison, Wisconsin, USA.
4. Sheldrick, G. M. (1997). *SHELXS '97* and *SHELXL '97*. University of Göttingen, Germany.
5. A.L.Spek (2005) PLATON, *A Multipurpose Crystallographic Tool*, Utrecht University, Utrecht, The Netherlands.

ZIF-1(CRB – Monoclinic)

Experimental and Refinement Details for ZIF-1

A colorless cubic crystal (0.15 × 0.10 × 0.10 mm^3) of ZIF-1 was placed in a 0.3 mm diameter borosilicate capillary along with a small amount of mother liquor, which was flame sealed, and mounted on a Bruker SMART APEX CCD diffractometer while being flash frozen to 223(2) K in a liquid N_2 cooled stream of nitrogen gas. Using 951 reflections chosen from the full data set, it was determined that the crystal was twinned by a rotation of 180º about the real axis [0.234 -0.935 1.000] (*CELL_NOW*; Sheldrick, 2004). Using the orientation matrices produced by this program, the data were reduced to F^2 values using the two-component version of *SAINT-Plus* (v. 7.0; Bruker, 2004). In the final refinement, the two-component reflection file was used with no averaging of equivalent reflections (including Friedel opposites). Integration of the data in the orthorhombic cell yielded a total of 41904 reflections of which 20536 were greater than 4σ(I). The range of θ was from 1.92 to 29.63º. Analysis of the data showed negligible decay during collection. The structure was solved in the monoclinic $P2_1/n$ space group with Z = 4 using direct methods. All non-hydrogen atoms were refined anisotropically with hydrogen atoms generated as spheres riding the coordinates of their parent atoms. Final full matrix least-squares refinement on F^2 converged to R_1 = 0.0423 (F >2σF))

and wR_2 = 0.0632 (all data) with GOF = 1.053. Most residual electron density in the final F-map was closely associated with the guest dimethylacetamide molecule within the pore of ZIF-1. However, the largest peak lies directly on Zn1, and is an artifact of refinement of structure with a twinned dataset.

Table S1. Crystal data and structure refinement for ZIF-1.

Empirical formula	C16 H21 N9 O Zn2	
Formula weight	486.16	
Temperature	223(2) K	
Wavelength	0.71073 Å	
Crystal system	Monoclinic	
Space group	P21/n	
Unit cell dimensions	a = 9.7405(19) Å	α= 90°.
	b = 15.266(3) Å	β= 98.62(3)°.
	c = 14.936(3) Å	γ = 90°.
Volume	2195.8(8) $Å^3$	
Z	4	
Density (calculated)	1.471 Mg/m^3	
Absorption coefficient	2.209 mm^{-1}	
F(000)	992	
Crystal size	0.15 x 0.10 x 0.10 mm^3	
Theta range for data collection	1.92 to 29.63°.	
Index ranges	-13<=h<=13, -21<=k<=21, -20<=l<=20	
Reflections collected	41776	
Independent reflections	41904 [R(int) = 0.0000]	
Completeness to theta = 29.63°	99.2 %	
Absorption correction	Semi-empirical from equivalents	
Max. and min. transmission	0.8093 and 0.7329	
Refinement method	Full-matrix least-squares on F^2	
Data / restraints / parameters	41904 / 0 / 257	
Goodness-of-fit on F^2	1.053	
Final R indices [I>2sigma(I)]	R1 = 0.0423, wR2 = 0.0603	
R indices (all data)	R1 = 0.0985, wR2 = 0.0632	
Largest diff. peak and hole	1.437 and -0.583 $e.Å^{-3}$	

Figure S2: ORTEP diagram of the Asymmetric Unit of ZIF-1 including dimethyl acetamide guest molecule.

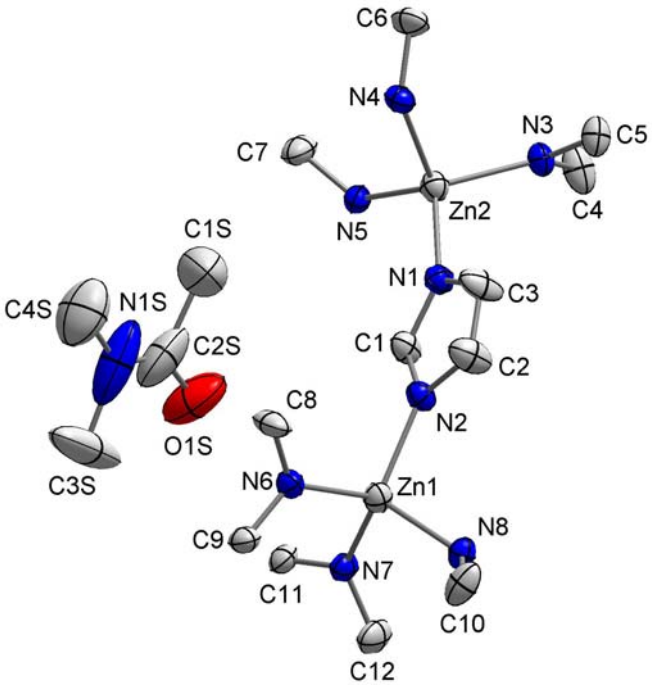

ZIF-2(CRB – Orthorhombic)

Experimental and Refinement Details for CRB – Orthorhombic

A colorless rod-shaped crystal (0.15 × 0.05 × 0.03 mm^3) of ZIF-2 was placed in a 0.3 mm diameter borosilicate capillary along with a small amount of mother liquor, which was flame sealed, and mounted on a Bruker SMART APEX CCD diffractometer while being flash frozen to 153(2) K in a liquid N_2 cooled stream of nitrogen gas. Integration of the data in the orthorhombic cell yielded a total of 12384 reflections of which 4094 were unique and 1936 were greater than $4\sigma(I)$. The range of θ was from 1.67 to 23.25º. Analysis of the data showed negligible decay during collection. The structure was solved in the monoclinic *P*bca space group with Z = 8 using direct methods. All non-hydrogen atoms were refined anisotropically with hydrogen atoms generated as spheres riding the coordinates of their parent atoms. Final full matrix least-squares refinement on F^2 converged to R_1 = 0.0591 ($F > 2\sigma F$)) and wR_2 = 0.1523 (all data) with GOF = 0.924. All residual electron density in the final F-map was closely associated with the guest dimethylformamide molecule within the pore of ZIF-2.

Table S2. Crystal data and structure refinement for ZIF-2.

Identification code	ZIF_CRB_Orthorhombic	
Empirical formula	C21 H12 N11 O3 Zn2	
Formula weight	597.16	
Temperature	153(2) K	
Wavelength	0.71073 Å	
Crystal system	Orthorhombic	
Space group	P b c a	
Unit cell dimensions	a = 9.679(3) Å	α= 90°.
	b = 24.114(6) Å	β= 90°.
	c = 24.450(6) Å	γ = 90°.
Volume	5707(3) $Å^3$	
Z	8	
Density (calculated)	1.390 Mg/m^3	
Absorption coefficient	1.722 mm^{-1}	
F(000)	2392	
Crystal size	0.15 x 0.05 x 0.03 mm^3	
Theta range for data collection	1.67 to 23.25°.	
Index ranges	-10<=h<=10, -26<=k<=19, -13<=l<=27	
Reflections collected	12384	
Independent reflections	4094 [R(int) = 0.0809]	
Completeness to theta = 23.25°	99.9 %	
Absorption correction	Semi-empirical from equivalents	
Max. and min. transmission	0.950 and 0.902	
Refinement method	Full-matrix least-squares on F^2	
Data / restraints / parameters	4094 / 0 / 334	
Goodness-of-fit on F^2	0.924	
Final R indices [I>2sigma(I)]	R1 = 0.0591, wR2 = 0.1299	
R indices (all data)	R1 = 0.1317, wR2 = 0.1523	
Largest diff. peak and hole	0.600 and -0.447 $e.Å^{-3}$	

Figure S3: ORTEP diagram of the asymmetric unit of ZIF-2 including guest dimethylformamide molecules. Ellipsoids are displayed at the 50 % probability level.

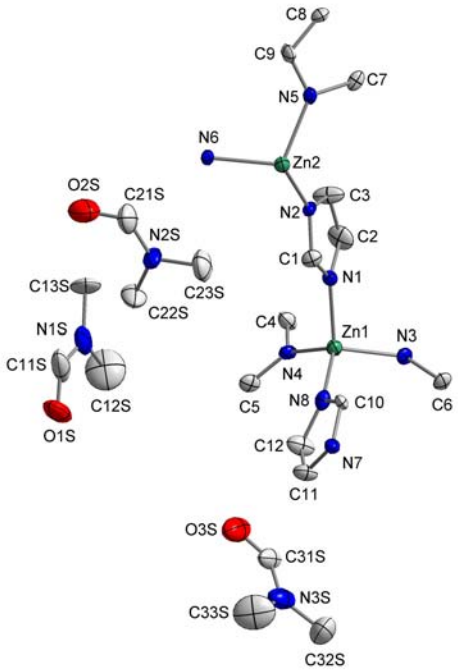

ZIF-3(DFT)

Experimental and Refinement Details for ZIF-3

A colorless prismatic crystal (0.20 × 0.20 × 0.15 mm^3) of ZIF-3 was placed in a 0.3 mm diameter borosilicate capillary along with a small amount of mother liquor, which was flame sealed, and mounted on a Bruker SMART APEX CCD diffractometer while being flash frozen to 258(2) K in a liquid N_2 cooled stream of nitrogen gas. Integration of the data in a primitive tetragonal cell yielded a total of 50492 reflections of which 3091 were unique and 1349 were greater than 4σ(*I*). The range of θ was from 1.62 to 25.72º. Analysis of the data showed negligible decay during collection. The structure was solved in the monoclinic $P4_2/mnm$ space group with Z = 16 using direct methods. All non-hydrogen atoms were refined anisotropically except for electron density within the pores which were modeled as isotropic oxygen atoms, hydrogen atoms were generated as spheres riding the coordinates of their parent atoms. Final full matrix least-squares refinement on F^2 converged to R_1 = 0.0610 ($F > 2\sigma F$)) and wR_2 = 0.1878 (all data) with GOF = 1.012. All residual electron density in the final F-map was closely associated with the guest molecules within the pore of ZIF-3.

Table S3. Crystal data and structure refinement for ZIF-3.

Empirical formula	C6 H6 N4 O3 Zn	
Formula weight	247.52	
Temperature	258(2) K	
Wavelength	0.71073 Å	
Crystal system	Tetragonal	
Space group	$P4_2/mnm$	
Unit cell dimensions	a = 18.9701(18) Å	α= 90°.
	b = 18.9701(18) Å	β= 90°.
	c = 16.740(3) Å	γ = 90°.
Volume	6024.3(14) $Å^3$	
Z	16	
Density (calculated)	1.092 Mg/m^3	
Absorption coefficient	1.622 mm^{-1}	
F(000)	1984	
Crystal size	0.20 x 0.20 x 0.15 mm^3	
Theta range for data collection	1.62 to 25.72°.	
Index ranges	-23<=h<=23, -23<=k<=23, -20<=l<=20	
Reflections collected	50942	
Independent reflections	3091 [R(int) = 0.1647]	
Completeness to theta = 25.72°	99.3 %	
Max. and min. transmission	0.7929 and 0.7373	
Refinement method	Full-matrix least-squares on F^2	
Data / restraints / parameters	3091 / 0 / 146	
Goodness-of-fit on F^2	1.012	
Final R indices [I>2sigma(I)]	R1 = 0.0610, wR2 = 0.1736	
R indices (all data)	R1 = 0.1293, wR2 = 0.1878	
Largest diff. peak and hole	0.963 and -0.485 $e.Å^{-3}$	

Figure S4: ORTEP diagram of the asymmetric unit of ZIF-3 framework.

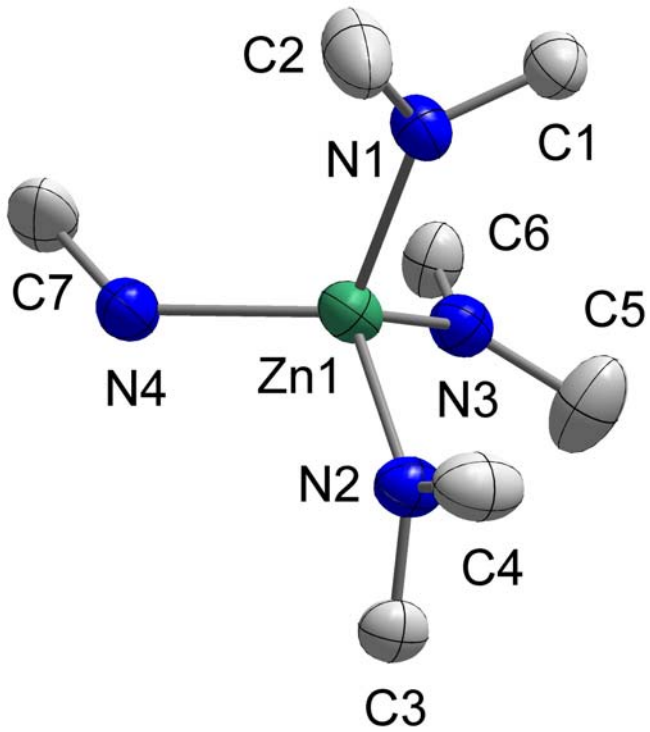

ZIF-4 (CAG)

Experimental and Refinement Details for ZIF-4

A colorless prismatic crystal (0.20 × 0.15 × 0.15 mm^3) of ZIF-4 was placed in a 0.3 mm diameter borosilicate capillary along with a small amount of mother liquor, which was flame sealed, and mounted on a Bruker SMART APEX CCD diffractometer while being flash frozen to 233(2) K in a liquid N_2 cooled stream of nitrogen gas. Integration of the data in the orthorhombic cell yielded a total of 45791 reflections of which 6074 were unique and 3960 were greater than 4σ(*I*). The range of θ was from 2.18 to 29.63º. Analysis of the data showed negligible decay during collection. The structure was solved in the monoclinic *P*bca space group with Z = 8 using direct methods. Atoms C4 and C9 were found to be disordered and with each group modeled as its own independent free variable. All non-hydrogen atoms were refined anisotropically with hydrogen atoms generated as spheres riding the coordinates of their parent atoms. Final full matrix least-squares refinement on F^2 converged to R_1 = 0.0406 ($F > 2\sigma F$)) and wR_2 = 0.1109 (all data) with GOF = 1.020. All residual electron density in the final F-map was closely associated with the guest dimethylformamide molecule within the pore of ZIF-4.

Table S4. Crystal data and structure refinement for ZIF-4.

Empirical formula	C15 H19 N9 O Zn2	
Formula weight	472.13	
Temperature	233(2) K	
Wavelength	0.71073 Å	
Crystal system	Orthorhombic	
Space group	Pbca	
Unit cell dimensions	a = 15.3950(17) Å	α= 90°.
	b = 15.3073(17) Å	β= 90°.
	c = 18.426(2) Å	γ = 90°.
Volume	4342.2(8) $Å^3$	
Z	8	
Density (calculated)	1.444 Mg/m^3	
Absorption coefficient	2.232 mm^{-1}	
F(000)	1920	
Crystal size	0.20 x 0.15 x 0.15 mm^3	
Theta range for data collection	2.18 to 29.63°.	
Index ranges	-21<=h<=21, -20<=k<=20, -25<=l<=25	
Reflections collected	45791	
Independent reflections	6074 [R(int) = 0.1045]	
Completeness to theta = 29.63°	99.2 %	
Absorption correction	Semi-empirical from equivalents	
Max. and min. transmission	0.7307 and 0.6638	
Refinement method	Full-matrix least-squares on F^2	
Data / restraints / parameters	6074 / 0 / 243	
Goodness-of-fit on F^2	1.020	
Final R indices [I>2sigma(I)]	R1 = 0.0406, wR2 = 0.1041	
R indices (all data)	R1 = 0.0682, wR2 = 0.1109	
Largest diff. peak and hole	0.575 and -0.483 $e.Å^{-3}$	

Figure S5: ORTEP diagram of the asymmetric unit of ZIF-4 including guest dimethylformamide molecule.

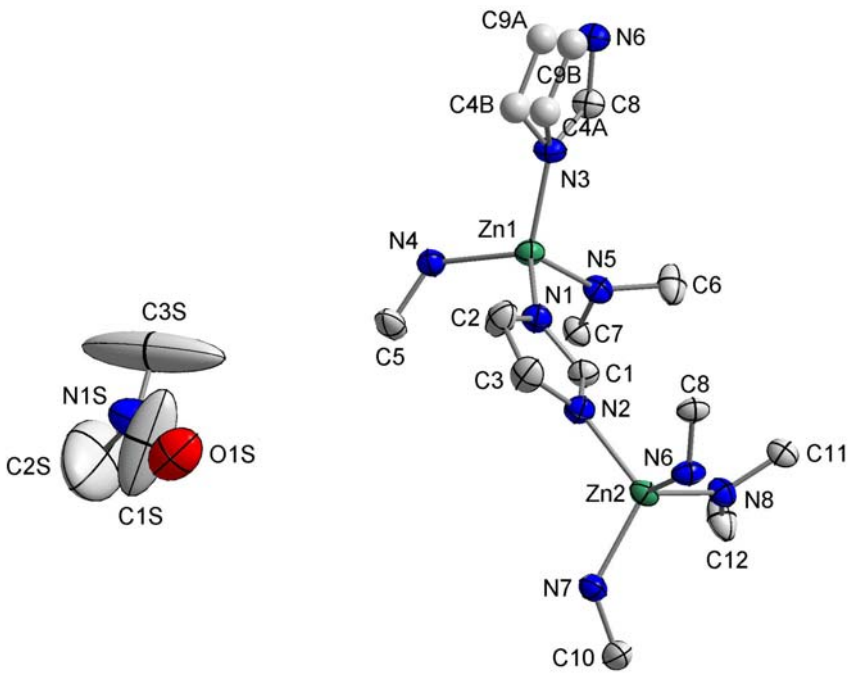

ZIF-5(GARNET)

Experimental and Refinement Details for ZIF-5

A colorless prism (0.15 × 0.12 × 0.10 mm^3) of ZIF-5 was placed in a 0.3 mm diameter borosilicate capillary along with a small amount of mother liquor, which was flame sealed, and mounted on a Bruker SMART APEX CCD diffractometer while being flash frozen to 196(2) K in a liquid N_2 cooled stream of nitrogen. A total of 35102 reflections were collected of which 1107 were unique and 997 were greater than $4\sigma(I)$. The range of θ was from 2.27 to 28.26º. Analysis of the data showed negligible decay during collection. The structure was solved in the cubic *I*a-3d space group with Z = 8 using direct methods. All non-hydrogen atoms were refined anisotropically with hydrogen atoms generated as spheres riding the coordinates of their parent atoms. Final full matrix least-squares refinement on F^2 converged to R_1 = 0.0191 ($F > 2\sigma F$)) and wR_2 = 0.0553 (all data) with GOF = 1.121.

Table S5. Crystal data and structure refinement for ZIF-5.

Empirical formula	C36 H36 In2 N24 Zn3	
Formula weight	1230.64	
Temperature	153(2) K	
Wavelength	0.71073 Å	
Crystal system	Cubic	
Space group	I a -3 d	
Unit cell dimensions	a = 21.9619(6) Å	α= 90°.
	b = 21.9619(6) Å	β= 90°.
	c = 21.9619(6) Å	γ = 90°.
Volume	10592.8(5) $Å^3$	
Z	8	
Density (calculated)	1.543 Mg/m^3	
Absorption coefficient	2.247 mm^{-1}	
F(000)	4864	
Crystal size	0.15 x 0.12 x 0.10 mm^3	
Theta range for data collection	2.27 to 28.26°.	
Index ranges	-29<=h<=27, -29<=k<=21, -29<=l<=25	
Reflections collected	35102	
Independent reflections	1107 [R(int) = 0.0245]	
Completeness to theta = 28.26°	100.0 %	
Absorption correction	Semi-empirical from equivalents	
Max. and min. transmission	0.799 and 0.703	
Refinement method	Full-matrix least-squares on F^2	
Data / restraints / parameters	1107 / 0 / 62	
Goodness-of-fit on F^2	1.121	
Final R indices [I>2sigma(I)]	R1 = 0.0191, wR2 = 0.0531	
R indices (all data)	R1 = 0.0221, wR2 = 0.0553	
Largest diff. peak and hole	0.762 and -0.155 $e.Å^{-3}$	

Figure S6: ORTEP diagram of the asymmetric unit of the ZIF-5 framework. Ellipsoids are displayed at the 50 % probability level.

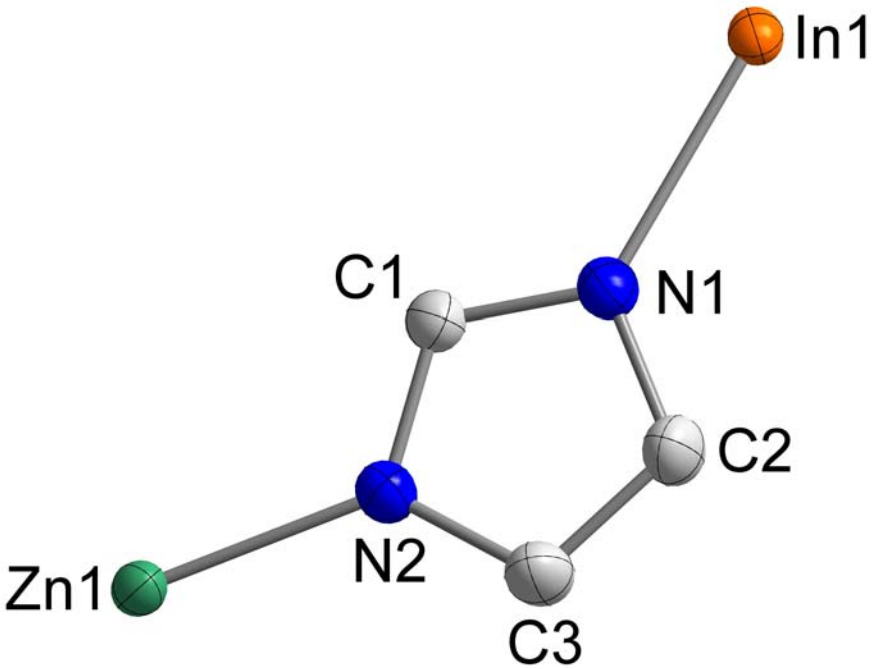

ZIF-6(GIS)

Experimental and Refinement Details for ZIF-6

A colorless block-shaped crystal (0.12 × 0.10 × 0.08 mm^3) of ZIF-6 was placed in a 0.3 mm diameter borosilicate capillary along with a small amount of mother liquor, which was flame sealed, and mounted on a Bruker SMART APEX CCD diffractometer while being flash frozen to 258(2) K in a liquid N_2 cooled stream of nitrogen 8840 reflections of which 1582 were unique and 821 were greater than 4σ(*I*). The range of θ was from 1.49 to 24.71º. Analysis of the data showed negligible decay during collection. The structure was solved in the monoclinic $I4_1/amd$ (origin choice No. 2) space group with Z = 16 using direct methods. Atoms C4A and C4B were the two components of a disordered carbon atom. The sof of C4A was refined as a free variable to converge at 0.53. Atoms C3A and C3B were two independent carbon atoms in an imidazole ring. This portion of the ring was disordered over two sites related by a two-fold axis. Therefore, the sofs of both C3A and C3B were fixed at 0.50. To treat the diffuse electron density, a protein diffuse scattering correction (SWAT) command was applied. The two variables g and U were refined to converge at 1.1 and 2.9, respectively. All non-hydrogen atoms were refined anisotropically with hydrogen atoms generated as

spheres riding the coordinates of their parent atoms. Final full matrix least-squares refinement on F^2 converged to $R_1 = 0.0642$ ($F > 2\sigma F$)) and $wR_2 = 0.2394$ (all data) with GOF = 1.013. All residual electron density in the final F-map was closely associated with the guest molecules within the pore of ZIF-6. Absorption corrections did not improve the quality of the data and was not applied.

Table S6. Crystal data and structure refinement for ZIF-6.

Identification code	GIS	
Empirical formula	C6 H6 N4 O0.50 Zn	
Formula weight	207.52	
Temperature	258(2) K	
Wavelength	0.71073 Å	
Crystal system	Tetragonal	
Space group	I4(1)/amd	
Unit cell dimensions	a = 18.515(3) Å	α= 90°.
	b = 18.515(3) Å	β= 90°.
	c = 20.245(4) Å	γ = 90°.
Volume	6940.2(19) $Å^3$	
Z	16	
Density (calculated)	0.794 Mg/m^3	
Absorption coefficient	1.390 mm^{-1}	
F(000)	1664	
Crystal size	0.12 x 0.10 x 0.08 mm^3	
Theta range for data collection	1.49 to 24.71°.	
Index ranges	-6<=h<=21, -21<=k<=20, -23<=l<=21	
Reflections collected	8840	
Independent reflections	1582 [R(int) = 0.0826]	
Completeness to theta = 24.71°	99.4 %	
Refinement method	Full-matrix least-squares on F^2	
Data / restraints / parameters	1582 / 0 / 58	
Goodness-of-fit on F^2	1.013	
Final R indices [I>2sigma(I)]	R1 = 0.0642, wR2 = 0.2260	
R indices (all data)	R1 = 0.1037, wR2 = 0.2394	
Largest diff. peak and hole	0.735 and -0.318 $e.Å^{-3}$	

Figure S7: ORTEP diagram for the asymmetric unit of the ZIF-6 framework.

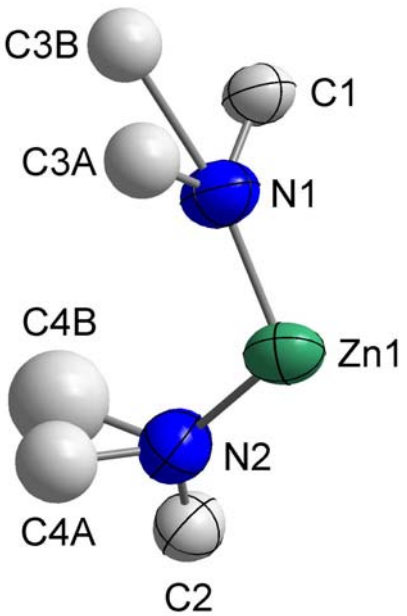

ZIF-7(SOD)

Experimental and Refinement Details for ZIF-7

A colorless prismatic crystal (0.10 × 0.07 × 0.05 mm^3) of ZIF-7 was placed in a 0.3 mm diameter borosilicate capillary along with a small amount of mother liquor, which was flame sealed, and mounted on a Bruker SMART APEX CCD diffractometer while being flash frozen to 233(2) K in a liquid N_2 cooled stream of nitrogen. A total of 8134 reflections were collected of which 4035 were unique and 1782 were greater than 4σ(*I*). The range of θ was from 1.65 to 29.55º. Analysis of the data showed negligible decay during collection. The structure was solved in the rhombohedral *R*-3 space group with Z = 18 using direct methods. All non-hydrogen atoms were refined anisotropically with hydrogen atoms generated as spheres riding the coordinates of their parent atoms. Final full matrix least-squares refinement on F^2 converged to R_1 = 0.0707 ($F > 2\sigma F$)) and wR_2 = 0.1270 (all data) with GOF = 1.038. All residual electron density in the final F-map was closely associated with the guest molecules within the pore of ZIF-7.

Table S7. Crystal data and structure refinement for ZIF-7.

Empirical formula	C14 H10 N4 O2.24 Zn	
Formula weight	335.47	
Temperature	258(2) K	
Wavelength	0.71073 Å	
Crystal system	Hexagonal	
Space group	R-3	
Unit cell dimensions	a = 22.989(3) Å	α= 90°.
	b = 22.989(3) Å	β= 90°.
	c = 15.763(3) Å	γ = 120°.
Volume	7214(2) $Å^3$	
Z	18	
Density (calculated)	1.390 Mg/m^3	
Absorption coefficient	1.542 mm^{-1}	
F(000)	3059	
Crystal size	0.10 x 0.07 x 0.05 mm^3	
Theta range for data collection	1.65 to 29.55°.	
Index ranges	-28<=h<=26, -26<=k<=14, -21<=l<=17	
Reflections collected	8134	
Independent reflections	4035 [R(int) = 0.0998]	
Completeness to theta = 29.55°	89.8 %	
Absorption correction	Semi-empirical from equivalents	
Max. and min. transmission	0.9269 and 0.8611	
Refinement method	Full-matrix least-squares on F^2	
Data / restraints / parameters	4035 / 0 / 195	
Goodness-of-fit on F^2	1.038	
Final R indices [I>2sigma(I)]	R1 = 0.0707, wR2 = 0.1157	
R indices (all data)	R1 = 0.1711, wR2 = 0.1270	
Largest diff. peak and hole	0.623 and -0.549 $e.Å^{-3}$	

Figure S8: ORTEP representation of the asymmetric unit of the ZIF-7 framework.

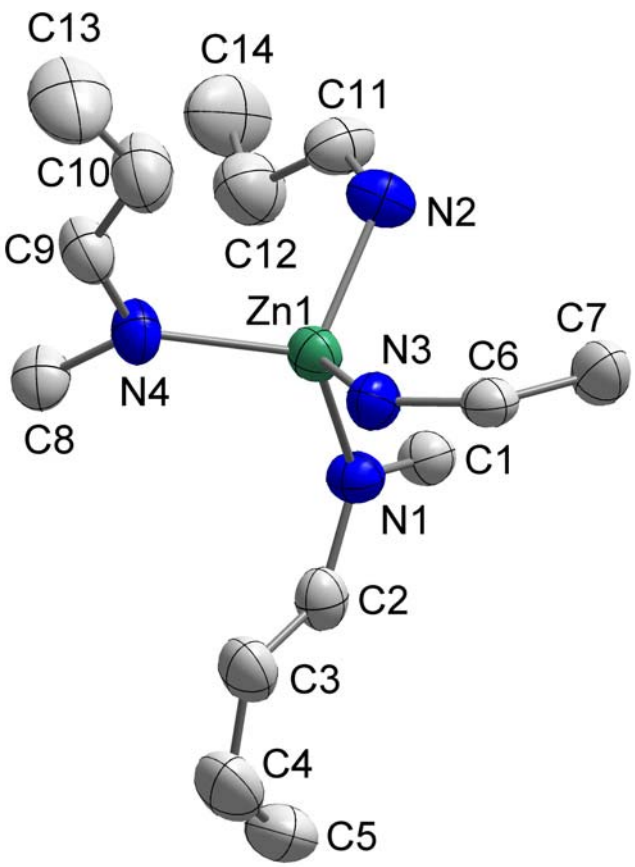

ZIF-8(SOD – Methyl Derivative)

Experimental and Refinement Details for ZIF-8

A colorless block crystal (0.16 × 0.10 × 0.10 mm^3) of ZIF-8 was placed in a 0.3 mm diameter borosilicate capillary along with a small amount of mother liquor, which was flame sealed, and mounted on a Bruker SMART APEX CCD diffractometer while being flash frozen to 258(2) K in a liquid N_2 cooled stream of nitrogen. A total of 27202 reflections were collected of which 1302 were unique and 1009 were greater than 4σ(*I*). The range of θ was from 2.94 to 29.61°. Analysis of the data showed negligible decay during collection. The structure was solved in the cubic *I*-43m space group with Z = 4 using direct methods. All non-hydrogen atoms were refined anisotropically with hydrogen atoms generated as spheres riding the coordinates of their parent atoms. Final full matrix least-squares refinement on F^2 converged to R_1 = 0.0314 ($F > 2\sigma F$)) and wR_2 = 0.0840 (all data) with GOF = 0.546. All residual electron density in the final F-map was closely associated with the guest molecules within the pore of ZIF-8.

Table S8. Crystal data and structure refinement for ZIF-8.

Empirical formula	C24 H30 N12 O10 Zn3	
Formula weight	842.71	
Temperature	258(2) K	
Wavelength	0.71073 Å	
Crystal system	Cubic	
Space group	I-43m	
Unit cell dimensions	a = 16.9910(12) Å	α= 90°.
	b = 16.9910(12) Å	β= 90°.
	c = 16.9910(12) Å	γ = 90°.
Volume	4905.2(6) $Å^3$	
Z	4	
Density (calculated)	1.141 Mg/m^3	
Absorption coefficient	1.503 mm^{-1}	
F(000)	1712	
Crystal size	0.16 x 0.10 x 0.10 mm^3	
Theta range for data collection	2.94 to 29.61°.	
Index ranges	-23<=h<=23, -23<=k<=23, -23<=l<=23	
Reflections collected	27202	
Independent reflections	1302 [R(int) = 0.0922]	
Completeness to theta = 29.61°	98.9 %	
Refinement method	Full-matrix least-squares on F^2	
Data / restraints / parameters	1302 / 0 / 46	
Goodness-of-fit on F^2	0.546	
Final R indices [I>2sigma(I)]	R1 = 0.0314, wR2 = 0.0758	
R indices (all data)	R1 = 0.0418, wR2 = 0.0840	
Absolute structure parameter	-0.01(2)	
Largest diff. peak and hole	0.428 and -0.216 $e.Å^{-3}$	

Figure S9: ORTEP diagram of the asymmetric unit of the ZIF-8 framework.

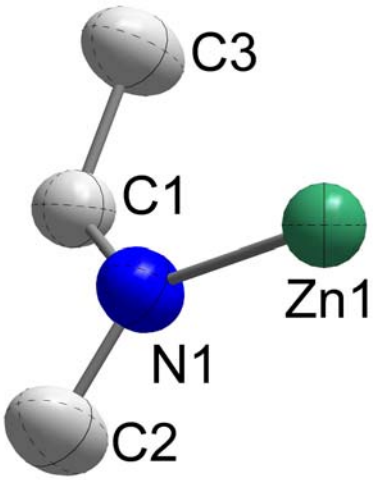

ZIF-9(SOD – Cobalt Form)

Experimental and Refinement Details for ZIF-9

A purple cubic crystal (0.17 × 0.17 × 0.17 mm^3) of ZIF-9 was placed in a 0.3 mm diameter borosilicate capillary along with a small amount of mother liquor, which was flame sealed, and mounted on a Bruker SMART APEX CCD diffractometer while being flash frozen to 233(2) K in a liquid N_2 cooled stream of nitrogen. A total of 24864 reflections were collected of which 3953 were unique and 2221were greater than 4σ(*I*). The range of θ was from 2.42 to 28.35º. Analysis of the data showed negligible decay during collection. The structure was solved in the rhombohedral *R*-3 space group with Z = 18 using direct methods. All non-hydrogen atoms were refined anisotropically with hydrogen atoms generated as spheres riding the coordinates of their parent atoms. Final full matrix least-squares refinement on F^2 converged to R_1 = 0.0979 ($F > 2\sigma F$)) and wR_2 = 0.2784 (all data) with GOF = 1.032. All residual electron density in the final F-map was closely associated with the guest molecules within the pore of ZIF-9.

Table S9. Crystal data and structure refinement for ZIF-9.

Empirical formula	C14 H10 N4 O2.24 Co	
Formula weight	251.89	
Temperature	258(2) K	
Wavelength	0.71073 Å	
Crystal system	Hexagonal	
Space group	R-3	
Unit cell dimensions	a = 22.9437(16) Å	α= 90°.
	b = 22.9437(16) Å	β= 90°.
	c = 15.747(2) Å	γ = 120°.
Volume	7178.8(12) $Å^3$	
Z	18	
Density (calculated)	1.398 Mg/m^3	
Absorption coefficient	1.089 mm^{-1}	
F(000)	3066	
Crystal size	0.17 x 0.17 x 0.17 mm^3	
Theta range for data collection	2.42 to 28.35°.	
Index ranges	-30<=h<=4, -16<=k<=25, -20<=l<=21	
Reflections collected	24864	
Independent reflections	3953 [R(int) = 0.1010]	
Completeness to theta = 28.35°	99.1 %	
Max. and min. transmission	0.8365 and 0.8365	
Refinement method	Full-matrix least-squares on F^2	
Data / restraints / parameters	3953 / 0 / 198	
Goodness-of-fit on F^2	1.032	
Final R indices [I>2sigma(I)]	R1 = 0.0979, wR2 = 0.2321	
R indices (all data)	R1 = 0.1700, wR2 = 0.2784	
Largest diff. peak and hole	0.726 and -0.727 $e.Å^{-3}$	

Figure S10: ORTEP diagram of the asymmetric unit of the ZIF-9 framework.

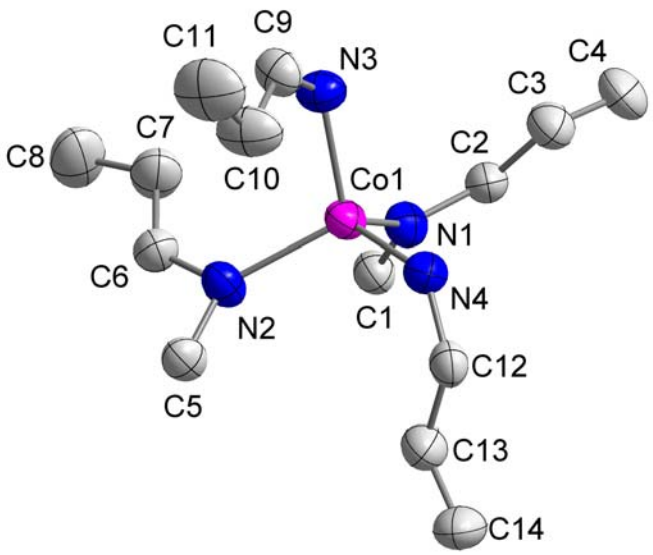

ZIF-10(MER)

Experimental and Refinement Details for ZIF-10

A colorless prismatic crystal (0.20 × 0.10 × 0.10 mm^3) of ZIF-10 was placed in a 0.3 mm diameter borosilicate capillary along with a small amount of mother liquor, which was flame sealed, and mounted on a Bruker SMART APEX CCD diffractometer while being flash frozen to 233(2) K in a liquid N_2 cooled stream of nitrogen. At total of 66076 reflections were collected of which 3376 were unique and 1771 were greater than 4σ(*I*). The range of θ was from 1.06 to 26.37º. Analysis of the data showed negligible decay during collection. The structure was solved in the monoclinic *I*4/mmm space group with Z = 32 using direct methods. Atoms C5 and C8 were found to be disordered and with each group modeled as its own independent free variable. All non-hydrogen atoms were refined anisotropically with hydrogen atoms generated as spheres riding the coordinates of their parent atoms. Final full matrix least-squares refinement on F^2 converged to R_1 = 0.0636 ($F > 2\sigma F$)) and wR_2 = 0.2457 (all data) with GOF = 1.059. All residual electron density in the final F-map was closely associated with the guest molecules within the pore of ZIF-10.

Table S10. Crystal data and structure refinement for ZIF-10.

Empirical formula	C6 H6 N4 O0.69 Zn	
Formula weight	210.52	
Temperature	223(2) K	
Wavelength	0.71073 Å	
Crystal system	Tetragonal	
Space group	I4/mmm	
Unit cell dimensions	a = 27.0608(18) Å	α= 90°.
	b = 27.0608(18) Å	β= 90°.
	c = 19.406(3) Å	γ = 90°.
Volume	14211(2) $Å^3$	
Z	32	
Density (calculated)	0.787 Mg/m^3	
Absorption coefficient	1.359 mm^{-1}	
F(000)	3376	
Crystal size	0.2 x 0.1 x 0.1 mm^3	
Theta range for data collection	1.06 to 26.37°.	
Index ranges	-33<=h<=33, -33<=k<=33, -24<=l<=24	
Reflections collected	66076	
Independent reflections	3998 [R(int) = 0.1371]	
Completeness to theta = 26.37°	99.2 %	
Absorption correction	Semi-empirical from equivalents	
Max. and min. transmission	0.873 and 0.850	
Refinement method	Full-matrix least-squares on F^2	
Data / restraints / parameters	3998 / 0 / 118	
Goodness-of-fit on F^2	1.059	
Final R indices [I>2sigma(I)]	R1 = 0.0636, wR2 = 0.2183	
R indices (all data)	R1 = 0.1291, wR2 = 0.2457	
Largest diff. peak and hole	0.557 and -0.501 $e.Å^{-3}$	

Figure S11: ORTEP diagram of the asymmetric unit of the ZIF-10 framework.

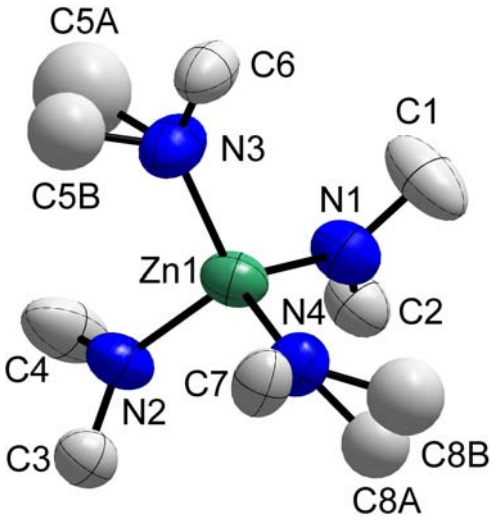

ZIF-11(RHO)

Experimental and Refinement Details for ZIF-11

A colorless cubic crystal (0.08 × 0.08 × 0.08 mm^3) of ZIF-11 was placed in a 0.3 mm diameter borosilicate capillary along with a small amount of mother liquor, which was flame sealed, and mounted on a Bruker SMART APEX CCD diffractometer while being flash frozen to 233(2) K in a liquid N_2 cooled stream of nitrogen. A total of 119088 reflections were collected of which 2415 were unique and 1300 were greater than 4σ(*I*). The range of θ was from 0.71 to 20.81º. Analysis of the data showed negligible decay during collection. The structure was solved in the cubic *P*m-3m space group with Z = 12 using direct methods. Atoms C7, C8, C12, C13, C14, and C16 were found to be disordered and with each group modeled as its own independent free variable. All non-hydrogen atoms were refined anisotropically with hydrogen atoms generated as spheres riding the coordinates of their parent atoms. To treat the diffuse electron density, a protein diffuse scattering correction (SWAT) command was applied. The two variables g and U were refined to converge at 1.1 and 3.6, respectively. Final full matrix least-squares refinement on F^2 converged to R_1 = 0.0778 (F >2σF)) and wR_2 = 0.2382 (all data) with GOF = 1.006. All residual electron density in the final F-map was closely associated with the guest molecules within the pore of ZIF-11.

Table S11. Crystal data and structure refinement for ZIF-11.

Empirical formula	C56 H40 N16 O3.77 Zn4	
Formula weight	1258.84	
Temperature	258(2) K	
Wavelength	0.71073 Å	
Crystal system	Cubic	
Space group	Pm-3m	
Unit cell dimensions	a = 28.7595(10) Å	α= 90°.
	b = 28.7595(10) Å	β= 90°.
	c = 28.7595(10) Å	γ = 90°.
Volume	23787.2(14) $Å^3$	
Z	12	
Density (calculated)	1.055 Mg/m^3	
Absorption coefficient	1.238 mm^{-1}	
F(000)	7658	
Crystal size	0.08 x 0.08 x 0.08 mm^3	
Theta range for data collection	0.71 to 20.81°.	
Index ranges	-28<=h<=28, -28<=k<=28, -28<=l<=28	
Reflections collected	119088	
Independent reflections	2415 [R(int) = 0.1688]	
Completeness to theta = 20.81°	96.8 %	
Max. and min. transmission	0.9074 and 0.9074	
Refinement method	Full-matrix least-squares on F^2	
Data / restraints / parameters	2415 / 3 / 195	
Goodness-of-fit on F^2	1.056	
Final R indices [I>2sigma(I)]	R1 = 0.0787, wR2 = 0.2246	
R indices (all data)	R1 = 0.1322, wR2 = 0.2498	
Largest diff. peak and hole	0.579 and -0.395 $e.Å^{-3}$	

Figure S12: ORTEP diagram of the asymmetric unit of the ZIF-11 framework.

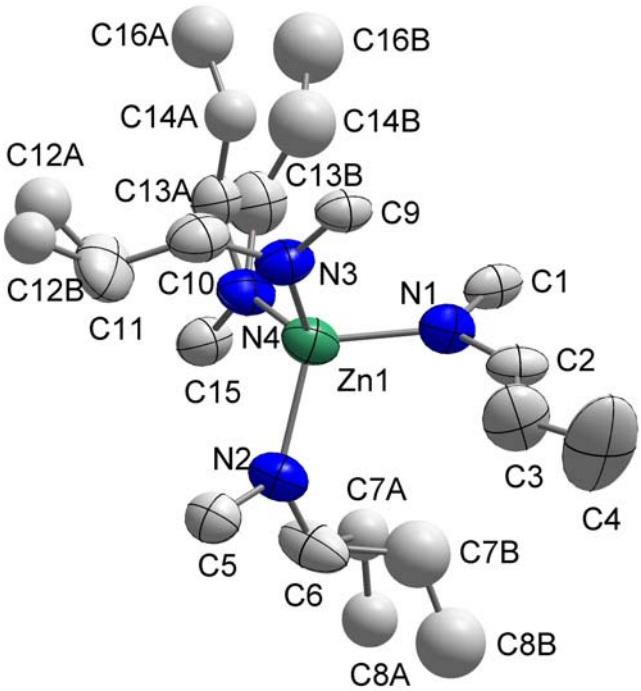

ZIF-12(RHO – Cobalt Form)

Experimental and Refinement Details for ZIF-12

A purple cubic crystal (0.08 × 0.08 × 0.08 mm^3) of ZIF-12 was placed in a 0.3 mm diameter borosilicate capillary along with a small amount of mother liquor, which was flame sealed, and mounted on a Bruker SMART APEX CCD diffractometer while being flash frozen to 233(2) K in a liquid N_2 cooled stream of nitrogen. A total of 21631 reflections were collected of which 1204 were unique and 398 were greater than 4σ(*I*). The range of θ was from 0.71 to 15.94º. Analysis of the data showed negligible decay during collection, however the amount of reliable data which could be collected was very limited due to the small crystal size of this sample and its lowered crystallinity. The structure was solved in the cubic *P*m-3m space group with Z = 12 using direct methods. Atoms C7, C8, C13, C14, and C16 were found to be disordered and with each group modeled as its own independent free variable. All non-hydrogen (except Co) and hydrogen atoms were refined isotropically with hydrogen atoms generated as spheres riding the coordinates of their parent atoms. Cobalt atoms was refined anisotropically. It should be noted that the precision of this model is low, and is reported to demonstrate that ZIF-12 can be isolated in crystalline form. Other supporting characterization data

(*vide infra* Materials and Methods) also support this conclusion. Final full matrix least-squares refinement on F^2 converged to R_1 = 0.1064 (F >2σF)) and wR_2 = 0.23712 (all data) with GOF = 1.202. All residual electron density in the final F-map was closely associated with the guest molecules within the pore of ZIF-12.

Table S12. Crystal data and structure refinement for ZIF-12.

Empirical formula	C13.58 H9.58 Co N4 O0.92	
Formula weight	280.176	
Temperature	258(2) K	
Wavelength	0.71073 Å	
Crystal system	Cubic	
Space group	Pm-3m	
Unit cell dimensions	a = 28.7595(10) Å	α= 90°.
	b = 28.7595(10) Å	β= 90°.
	c = 28.7595(10) Å	γ = 90°.
Volume	23787.2(14) $Å^3$	
Z	12	
Density (calculated)	1.014 Mg/m^3	
Absorption coefficient	0.864 mm^{-1}	
F(000)	7366	
Crystal size	0.08 x 0.08 x 0.08 mm^3	
Theta range for data collection	1.00 to 15.94°.	
Index ranges	-16<=h<=22, -21<=k<=21, -22<=l<=16	
Reflections collected	21631	
Independent reflections	1204 [R(int) = 0.4632]	
Completeness to theta = 15.94°	99.0 %	
Absorption correction	Semi-empirical from equivalents	
Max. and min. transmission	0.9341 and 0.9341	
Refinement method	Full-matrix least-squares on F^2	
Data / restraints / parameters	1204 / 8 / 124	
Goodness-of-fit on F^2	1.202	
Final R indices [I>2sigma(I)]	R1 = 0.1064, wR2 = 0.3393	
R indices (all data)	R1 = 0.2328, wR2 = 0.3712	
Largest diff. peak and hole	0.907 and -0.439 $e.Å^{-3}$	

Figure S13: ORTEP diagram of the asymmetric unit of the ZIF-12 framework. Note only Co has been refined anisotropically.

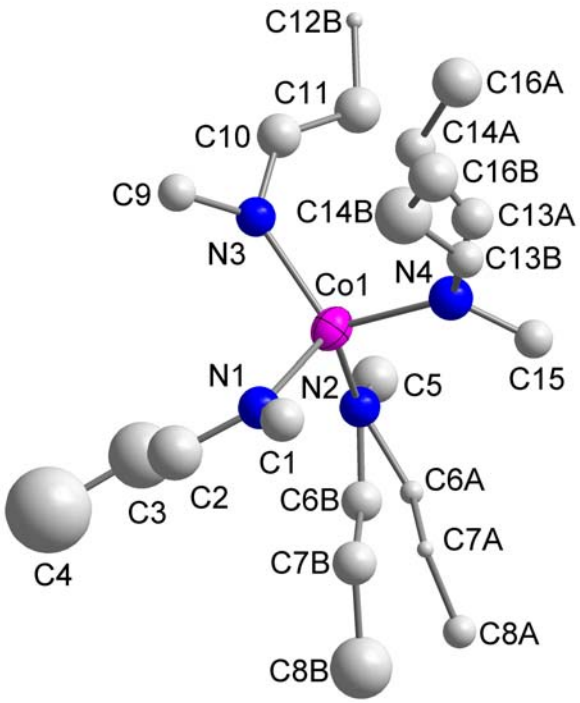

Section S3. Experimental and Simulated PXRD Patterns

Powder X-ray diffraction (PXRD) data were collected using a Bruker D8-Advance θ-2θ diffractometer in reflectance Bragg-Brentano geometry employing Ni filtered Cu Kα line focused radiation at 1600 W (40kV, 40 mA) power and equipped with a Na(Tl) scintillation detector fitted a 0.2 mm radiation entrance slit. All samples were ground to ensure mono-dispersity in the bulk, then mounted onto a zero-background sample holder by dropping powders from a wide-blade spatula and then leveling the sample surface with a razor blade. The best counting statistics were achieved by using a 0.02º 2θ step scan from 1.5 – 60º with an exposure time of 10 s per step.

In this section, we report the experimental PXRD patterns of ZIF-1, -4, -7, -8 and –11, and the comparison with PXRD patterns simulated from the single crystal structures of these compounds.

Figure S14. Comparison of the experimental PXRD pattern of as-prepared ZIF-1 (top) with the one simulated from its single crystal structure (bottom). The very high degree of correspondence between the patterns indicates that the bulk material has the same structure as the single crystal.

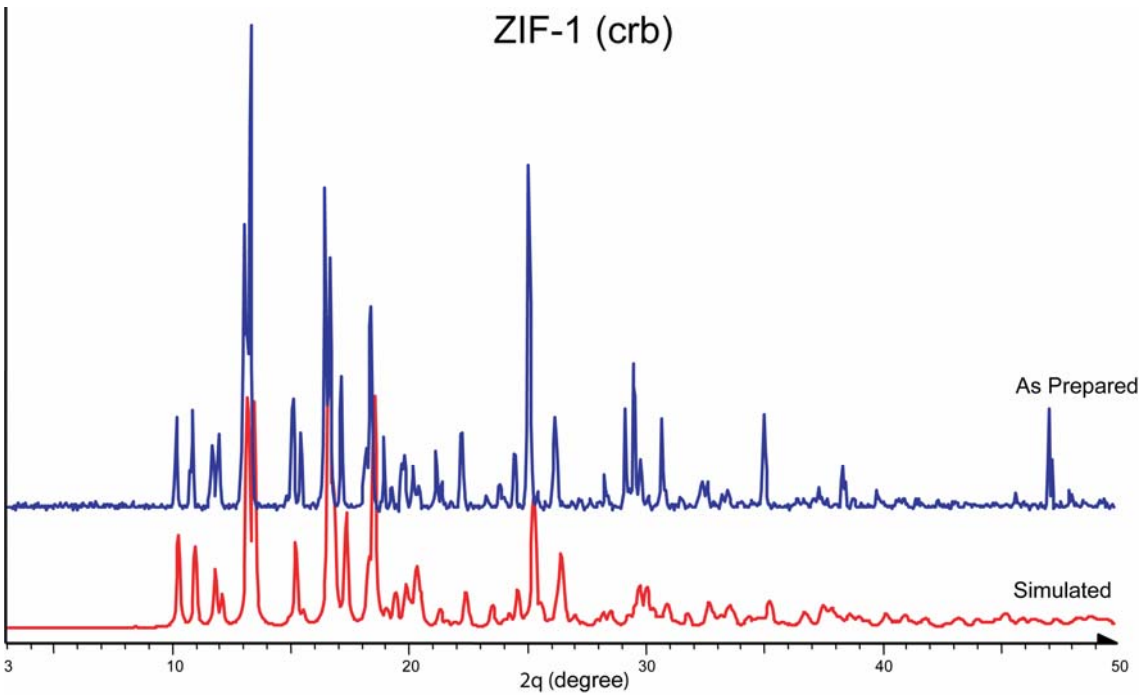

Table S13. Comparison of positions and indices of diffraction lines in the experimental and simulated PXRD patterns of ZIF-1(crb). Deviations from perfect correspondence primarily arise from difference in data collection temperatures (cryogenic for single crystal data and room temperature for bulk powder).

Observed PXRD		Simulated PXRD		Indices
2-Theta	d	2-Theta	d	hkl
10.16	8.698	10.18	8.684	-101
11.19	7.899	11.71	7.548	-1-11
11.93	7.384	11.98	7.384	002
12.96	6.825	13.05	6.781	021
13.26	6.674	13.31	6.647	012
15.02	5.893	15.12	5.852	-112
15.39	5.753	15.44	5.733	-1-21
16.42	5.394	16.48	5.373	121
16.64	5.323	16.69	5.307	022
17.23	5.142	17.19	5.155	112
18.34	4.835	18.41	4.815	200
25.04	3.554	25.08	3.548	140

Figure S15. Comparison of the experimental PXRD pattern of as-prepared ZIF-4 (top) with the one simulated from its single crystal structure (bottom). The very high degree of correspondence between the patterns indicates that the bulk material has the same structure as the single crystal.

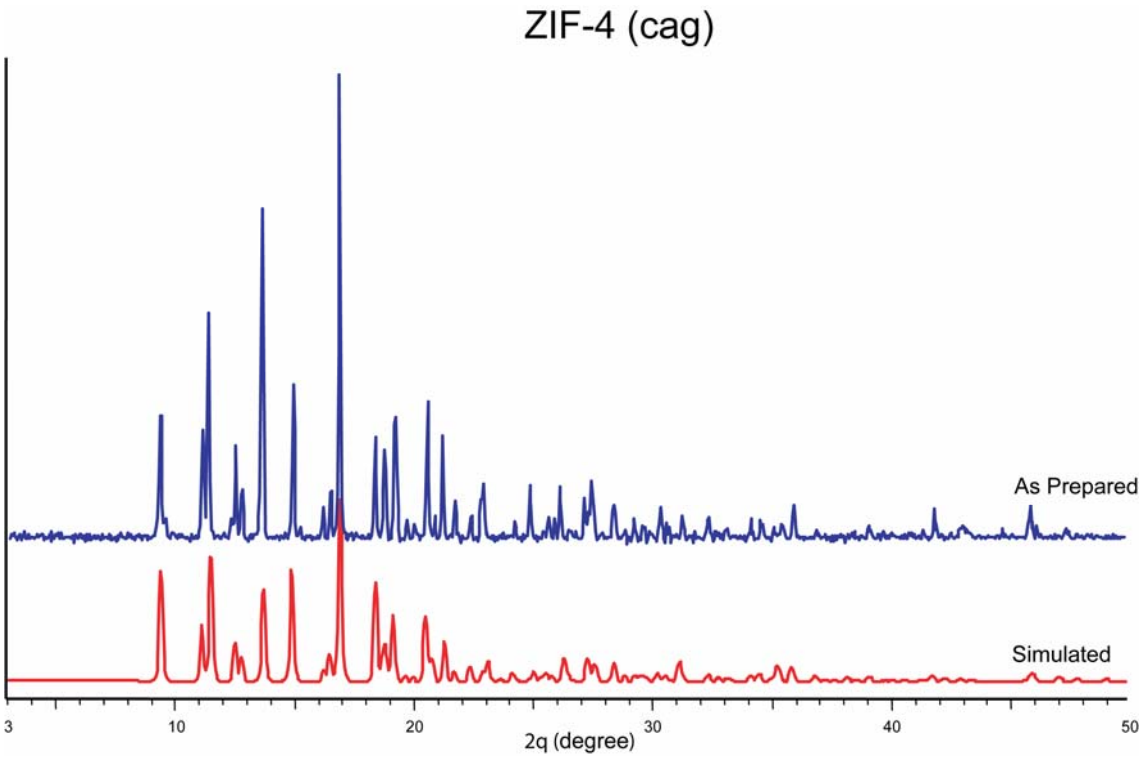

Table S14. Comparison of positions and indices of diffraction lines in the experimental and simulated PXRD patterns of ZIF-4 (cag). Deviations from perfect correspondence primarily arise from difference in data collection temperatures (cryogenic for single crystal data and room temperature for bulk powder).

Observed PXRD		Simulated PXRD		Indices
2-Theta	d	2-Theta	d	hkl
9.38	9.420	9.45	9.353	111
11.03	8.019	11.18	7.906	102
11.37	7.778	11.55	7.654	020
12.53	7.058	12.51	7.068	021
12.60	7.020	12.59	7.024	112
13.63	6.493	13.77	6.423	121
14.86	5.957	14.98	5.907	202
16.09	5.503	16.07	5.511	212
16.50	5.367	16.57	5.345	113
16.84	5.259	17.01	5.206	221
18.22	4.866	18.51	4.790	023
18.76	4.726	18.85	4.704	311
19.24	4.609	19.25	4.606	004

Figure S16. Comparison of the experimental PXRD pattern of as-prepared ZIF-7 (top) with the one simulated from its single crystal structure (bottom). The very high degree of correspondence between the patterns indicates that the bulk material has the same structure as the single crystal.

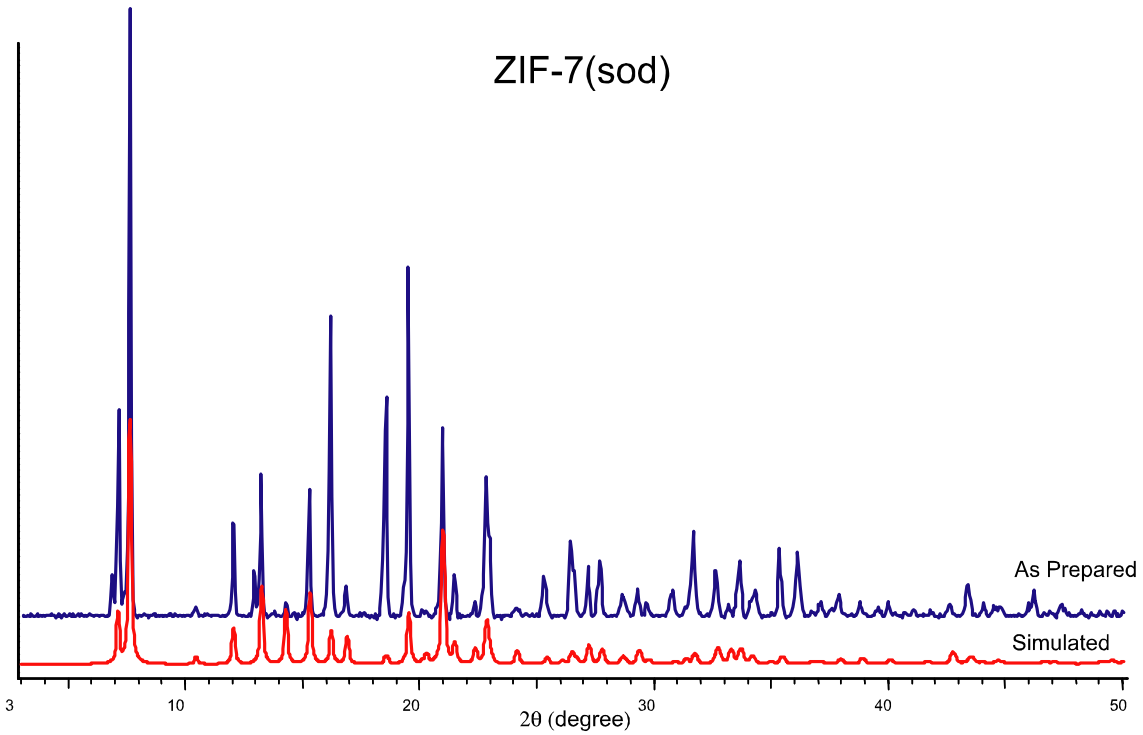

Table S15. Comparison of positions and indices of diffraction lines in the experimental and simulated PXRD patterns of ZIF-7 (sod). Deviations from perfect correspondence primarily arise from difference in data collection temperatures (cryogenic for single crystal data and room temperature for bulk powder).

Observed PXRD		Simulated PXRD		Indices
2-Theta	d	2-Theta	d	hkl
7.12	12.413	7.14	12.358	-111
7.60	11.629	7.68	11.494	110
12.16	7.271	12.07	7.329	012
13.21	6.691	13.33	6.636	030
15.29	5.791	15.41	5.747	220
16.25	5.450	16.27	5.443	-132
18.61	4.765	18.55	4.779	113
19.57	4.533	19.61	4.522	312
21.11	4.206	21.09	4.208	042
21.64	4.104	21.55	4.119	-333
22.93	3.875	22.91	3.878	-243
31.78	2.814	31.87	2.806	-663

Figure S17. Comparison of the experimental PXRD pattern of as-prepared ZIF-8 (top) with the one simulated from its single crystal structure (bottom). The very high degree of correspondence between the patterns indicates that the bulk material has the same structure as the single crystal.

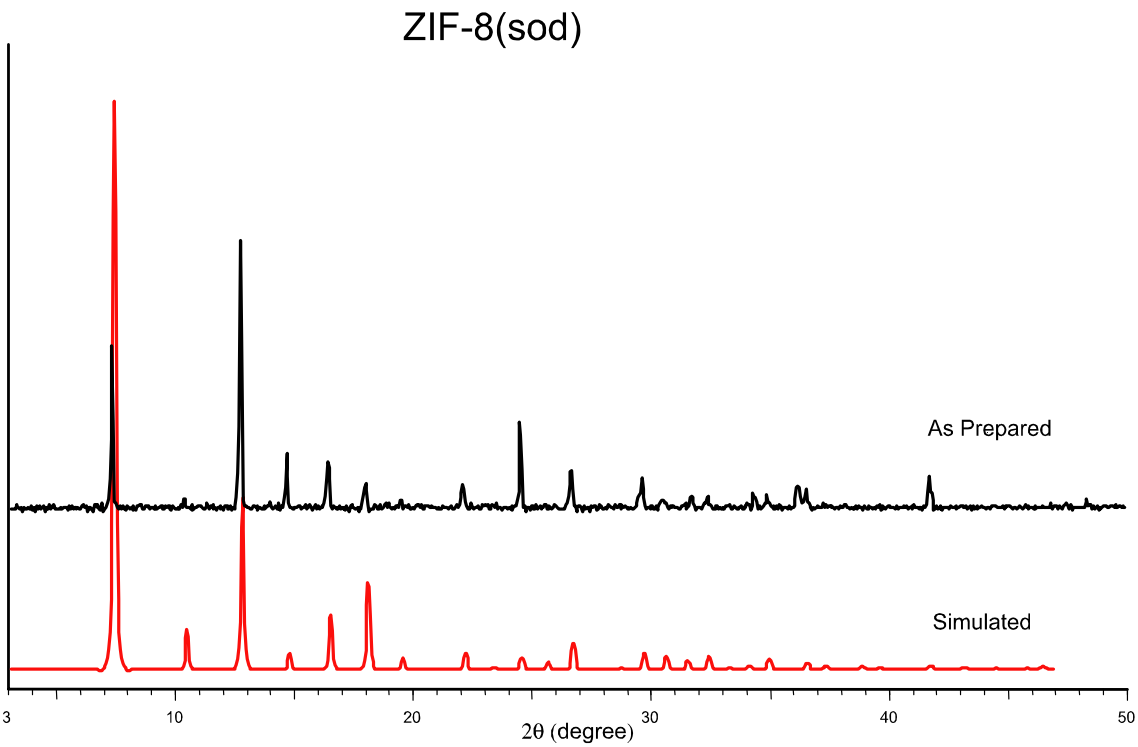

Table S16. Comparison of positions and indices of diffraction lines in the experimental and simulated PXRD patterns of ZIF-8 (sod). Deviations from perfect correspondence primarily arise from difference in data collection temperatures (cryogenic for single crystal data and room temperature for bulk powder).

Observed PXRD		Simulated PXRD		Indices
2-Theta	d	2-Theta	d	hkl
7.31	12.085	7.35	12.015	011
10.24	8.629	10.40	8.496	002
12.65	6.994	12.75	6.937	112
14.67	6.035	14.73	6.007	022
16.03	5.433	16.48	5.373	013
17.84	4.905	18.07	4.905	222
22.02	4.033	22.18	4.005	114
24.38	3.648	24.55	3.623	233
26.64	3.343	26.73	3.332	134
29.72	3.004	29.72	3.004	044
30.44	2.934	30.65	2.914	334
31.69	2.821	31.57	2.832	244
32.41	2.760	32.46	2.756	235

Figure S18. Comparison of the experimental PXRD pattern of as-prepared ZIF-11 (top) with the one simulated from its single crystal structure (bottom). The very high degree of correspondence between the patterns indicates that the bulk material has the same structure as the single crystal.

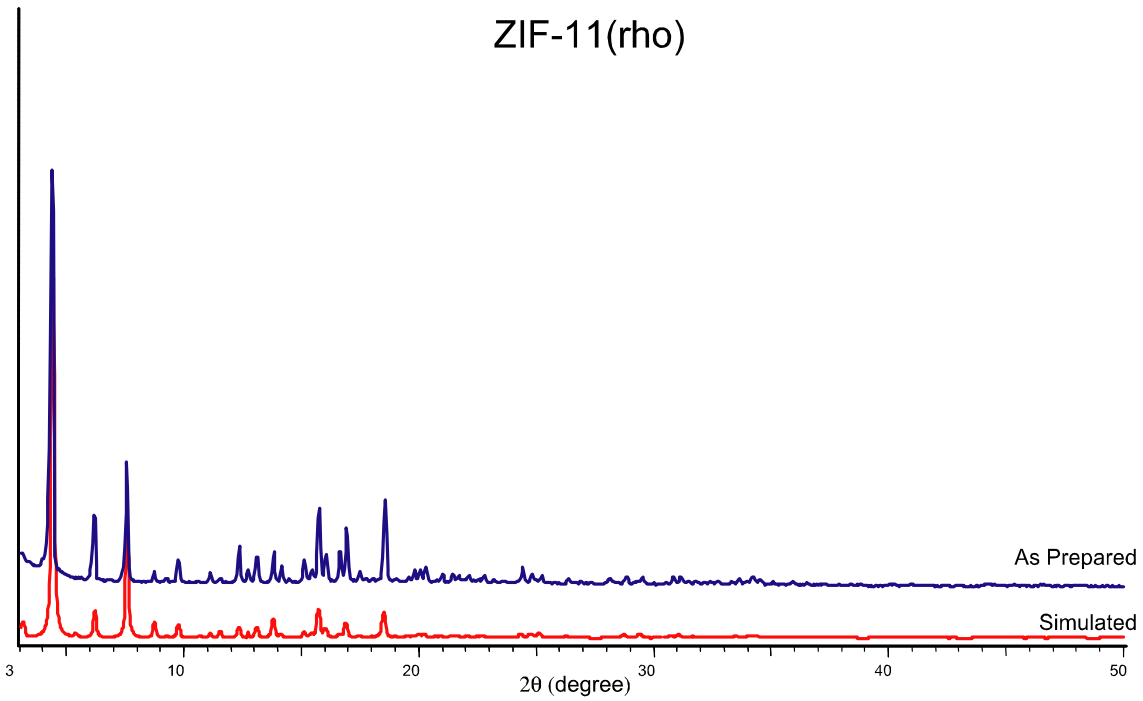

Table S17. Comparison of positions and indices of diffraction lines in the experimental and simulated PXRD patterns of ZIF-11 (rho). Deviations from perfect correspondence primarily arise from difference in data collection temperatures (cryogenic for single crystal data and room temperature for bulk powder).

Observed PXRD		Simulated PXRD		Indices
2-Theta	d	2-Theta	d	Hkl
3.09	28.564	3.07	28.759	001
4.31	20.466	4.34	20.336	011
6.03	14.655	6.14	14.380	002
7.53	11.727	7.52	11.741	112
8.63	10.240	8.69	10.168	022
9.72	9.089	9.72	9.095	013
11.09	7.970	11.08	7.977	023
12.33	7.175	12.30	7.190	004
12.74	6.945	12.68	6.975	223
13.01	6.799	13.05	6.779	033
13.83	6.3971	13.76	6.431	024
15.75	5.622	15.70	5.640	015
17.05	5.196	17.42	5.084	044
18.42	4.813	18.50	4.793	006

Section S4. Chemical Stability Tests

ZIF-7, 8, and 11 were tested for their stability in benzene, methanol and water. These solvents were chosen to compare the relative effects of non-polar to polar solvents. The tests were performed at room temperature, 50 °C and at the boiling point of each solvent (methanol 65 °C, benzene 80 °C and water 100 °C) for up to 7 days. The structural stability of the frameworks were monitored by aliquoting portions of the samples for PXRD analysis after every 24 h period.

Figure S19. PXRD patterns of ZIF-7 collected during stability test in benzene at room temperature. The framework structure of ZIF-7 was unchanged after 7 days.

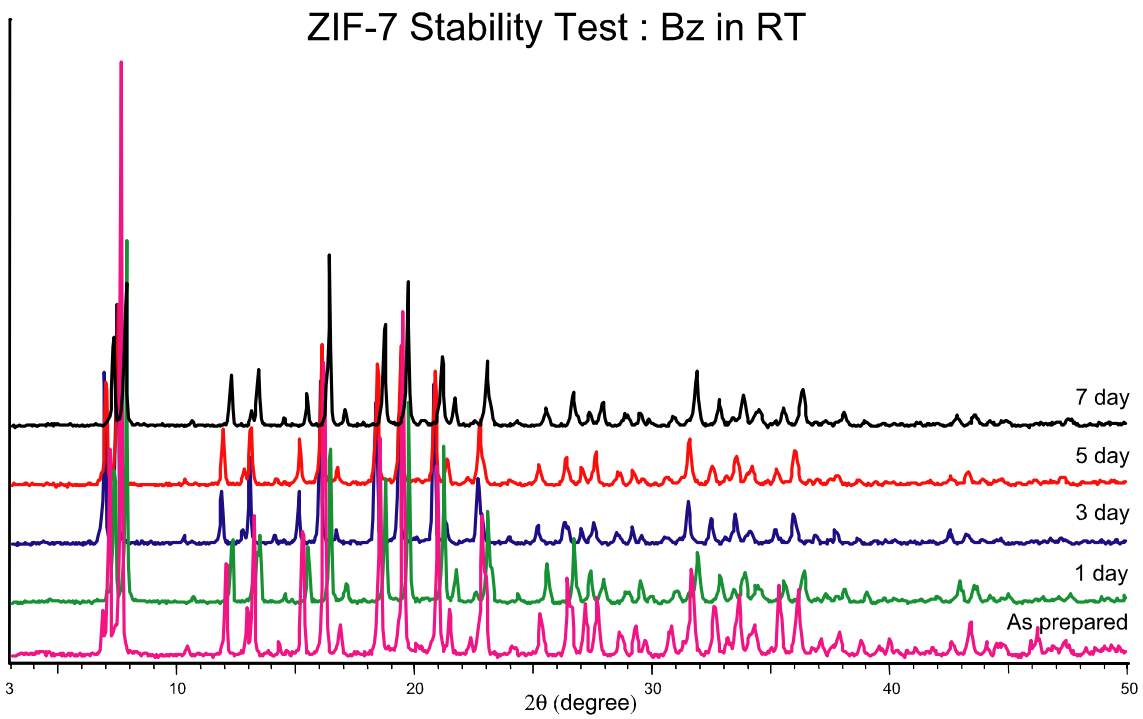

Figure S20. PXRD patterns of ZIF-7 collected during stability test in benzene at 50°C. The framework structure of ZIF-7 was unchanged after 7 days.

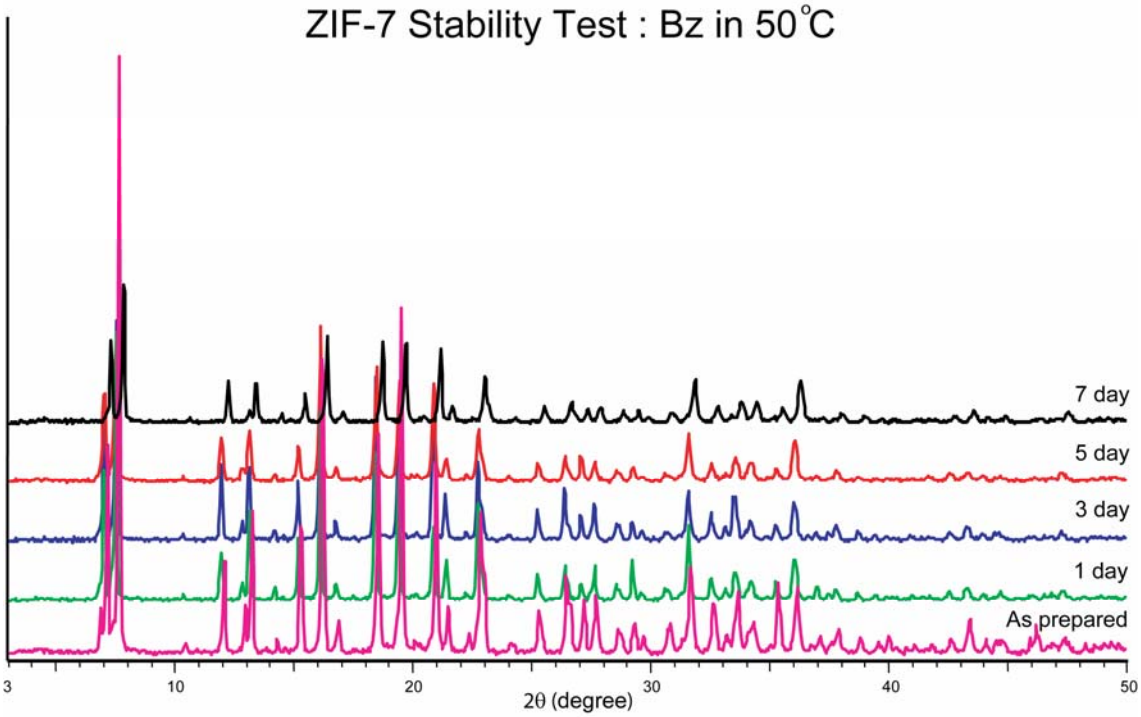

Figure S21. PXRD patterns of ZIF-7 collected during stability test in refluxing benzene. The framework structure of ZIF-7 was unchanged after 7 days.

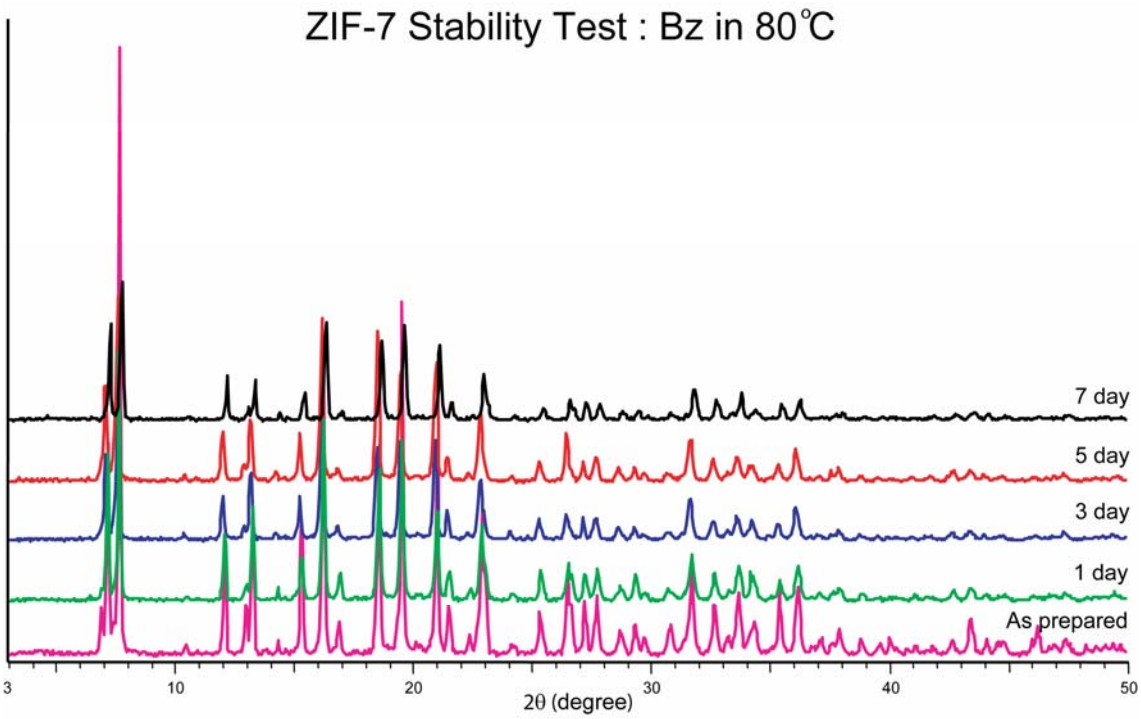

Figure S22. PXRD patterns of ZIF-7 collected during stability test in methanol at room temperature. The framework structure of ZIF-7 was unchanged after 7 days.

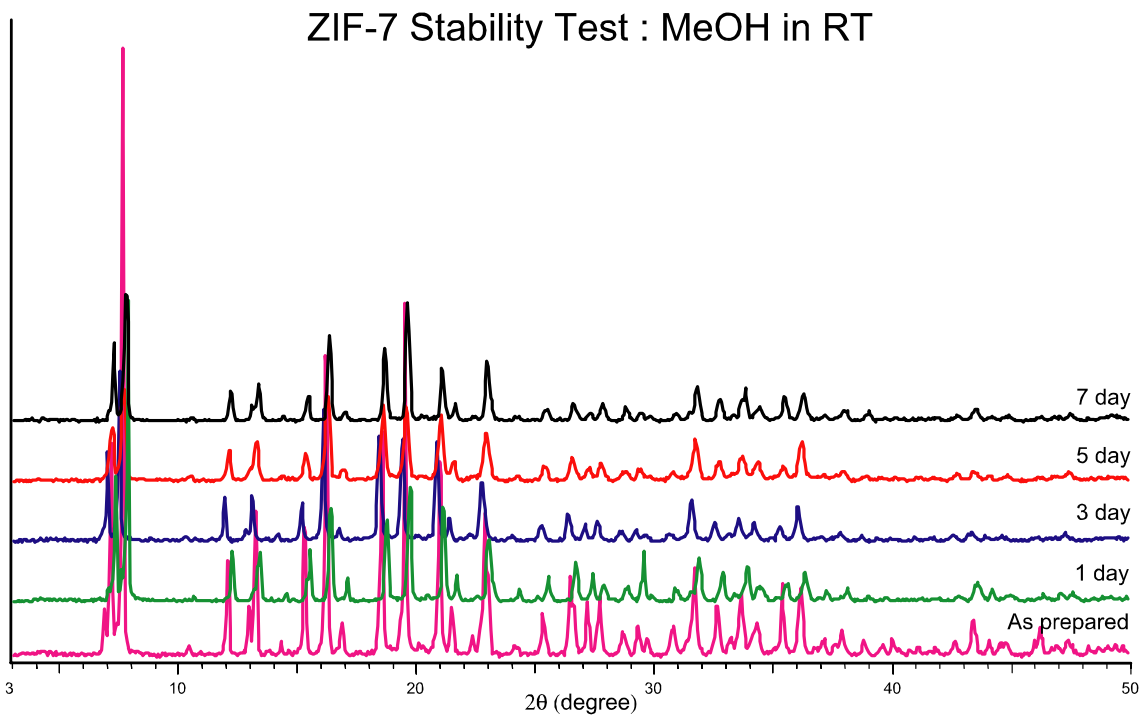

Figure S23. PXRD patterns of ZIF-7 collected during stability test in methanol at 50°C. The framework structure of ZIF-7 was unchanged after 7 days.

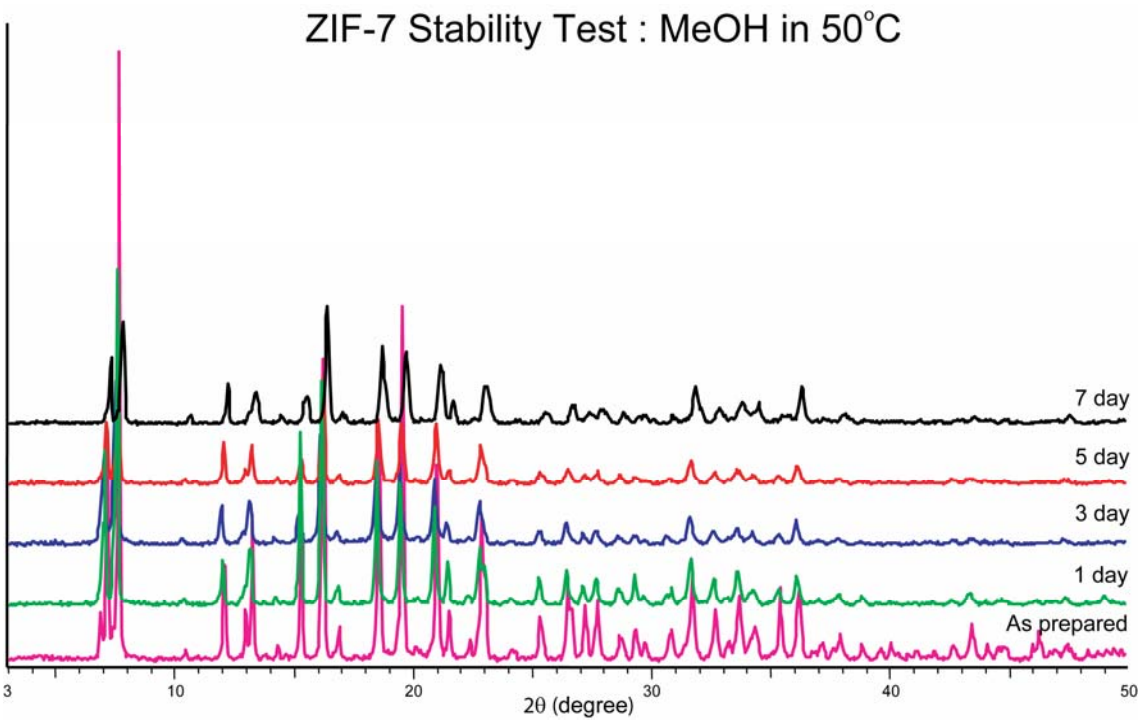

Figure S24. PXRD patterns of ZIF-7 collected during stability test in refluxing methanol. The framework structure of ZIF-7 was unchanged after 7 days.

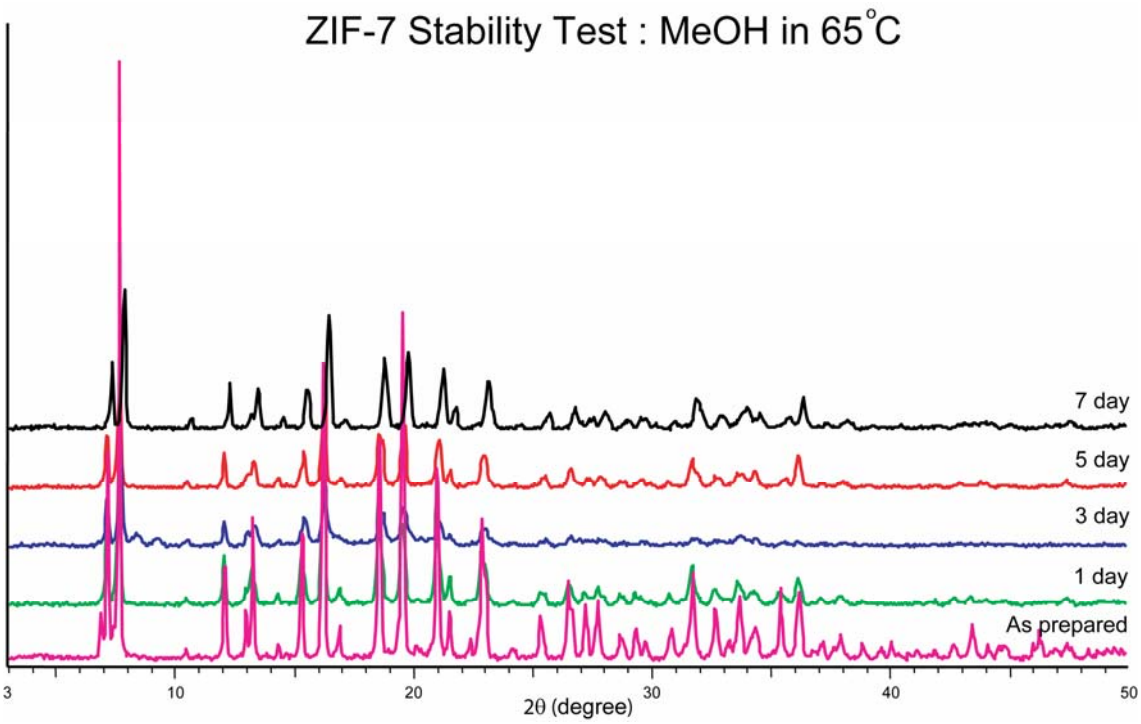

Figure S25. PXRD patterns of ZIF-7 collected during stability test in water at room temperature. The framework structure of ZIF-7 was unchanged after 7 days.

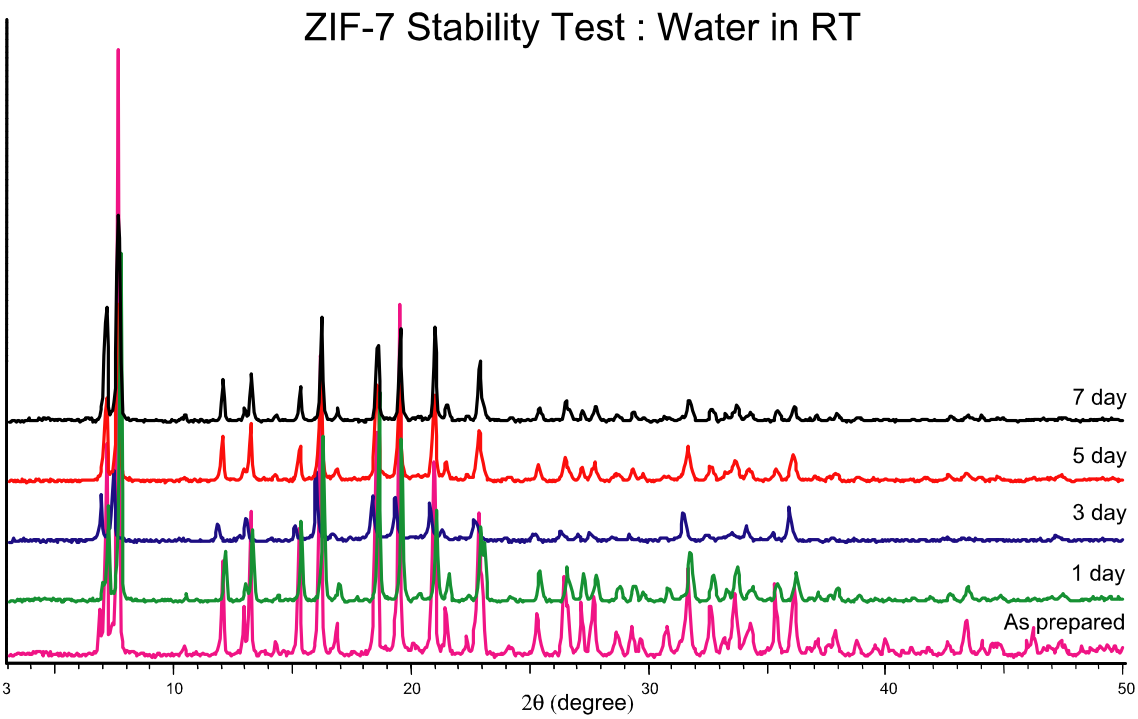

Figure S26. PXRD patterns of ZIF-7 collected during stability test in water at 50°C. The framework structure of ZIF-7 was unchanged after 7 days.

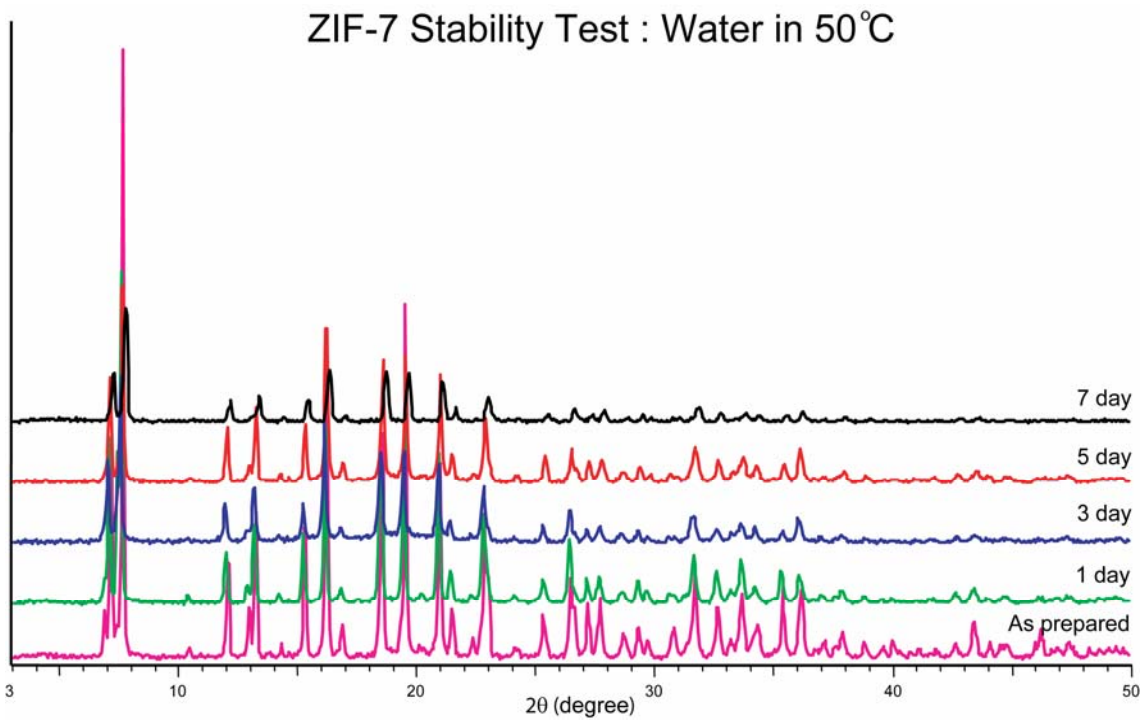

Figure S27. PXRD patterns of ZIF-7 collected during stability test in refluxing water. ZIF-7 was transformed to another crystalline material after 1 day.

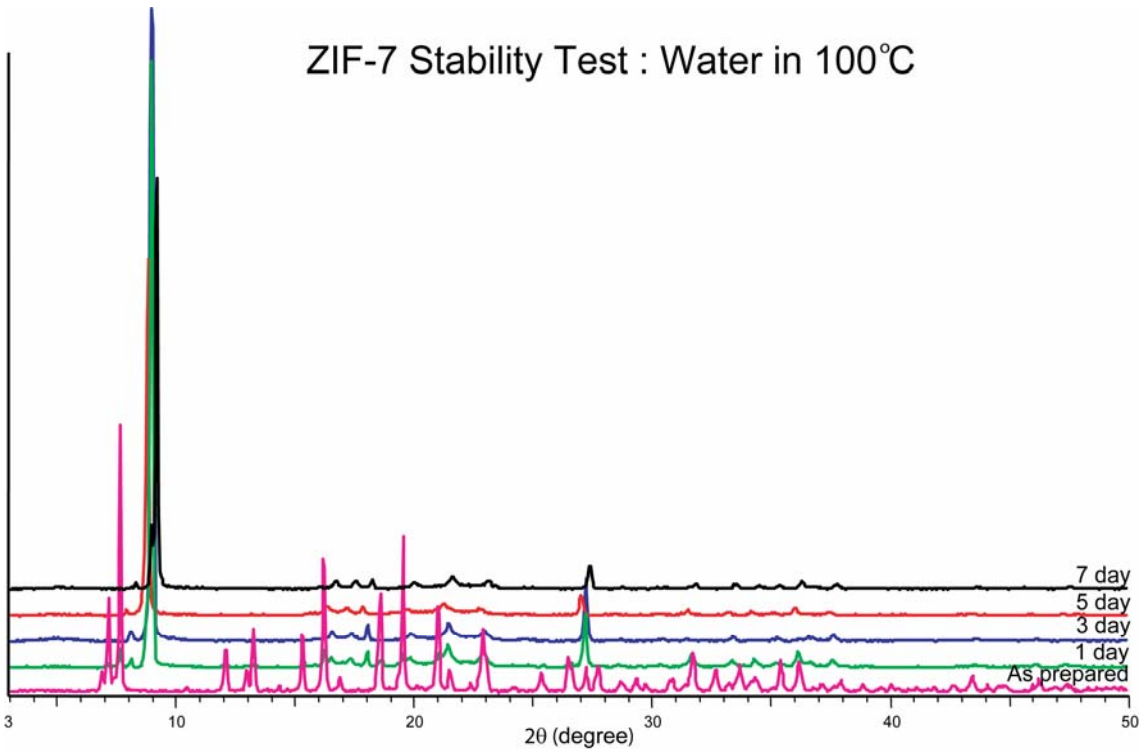

Figure S28. PXRD patterns of ZIF-8 collected during stability test in benzene at room temperature. The framework structure of ZIF-8 was unchanged after 7 days.

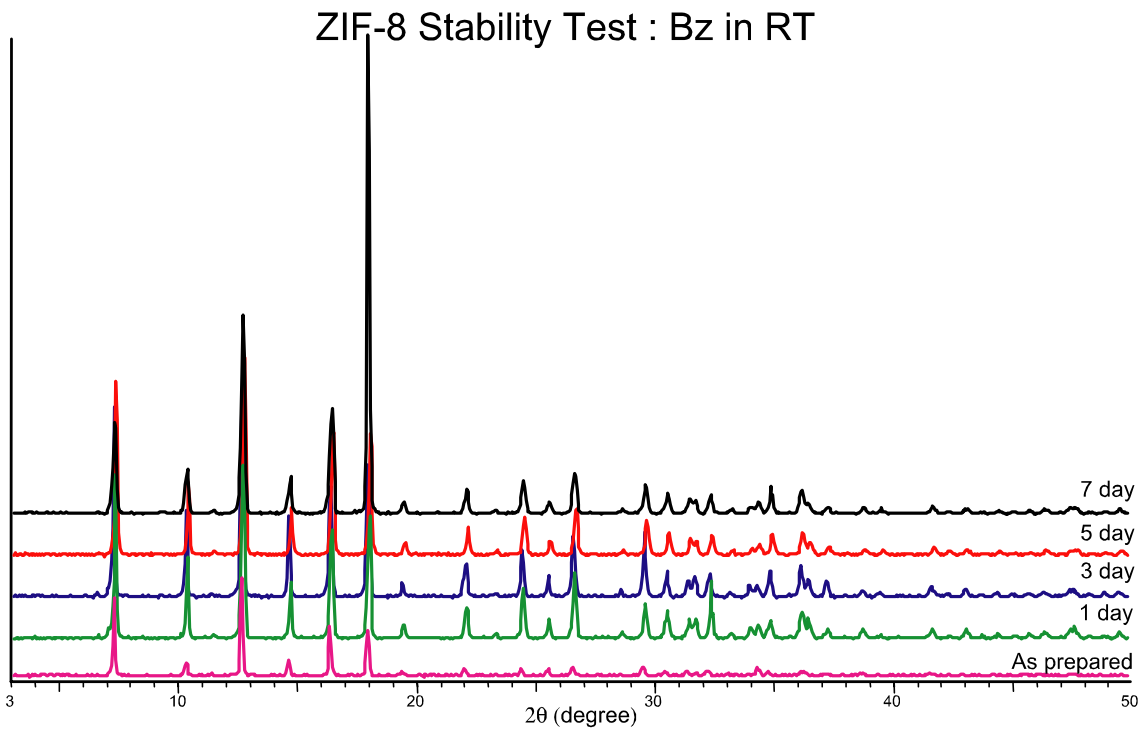

Figure S29. PXRD patterns of ZIF-8 collected during stability test in benzene at 50°C. The framework structure of ZIF-8 was unchanged after 7 days.

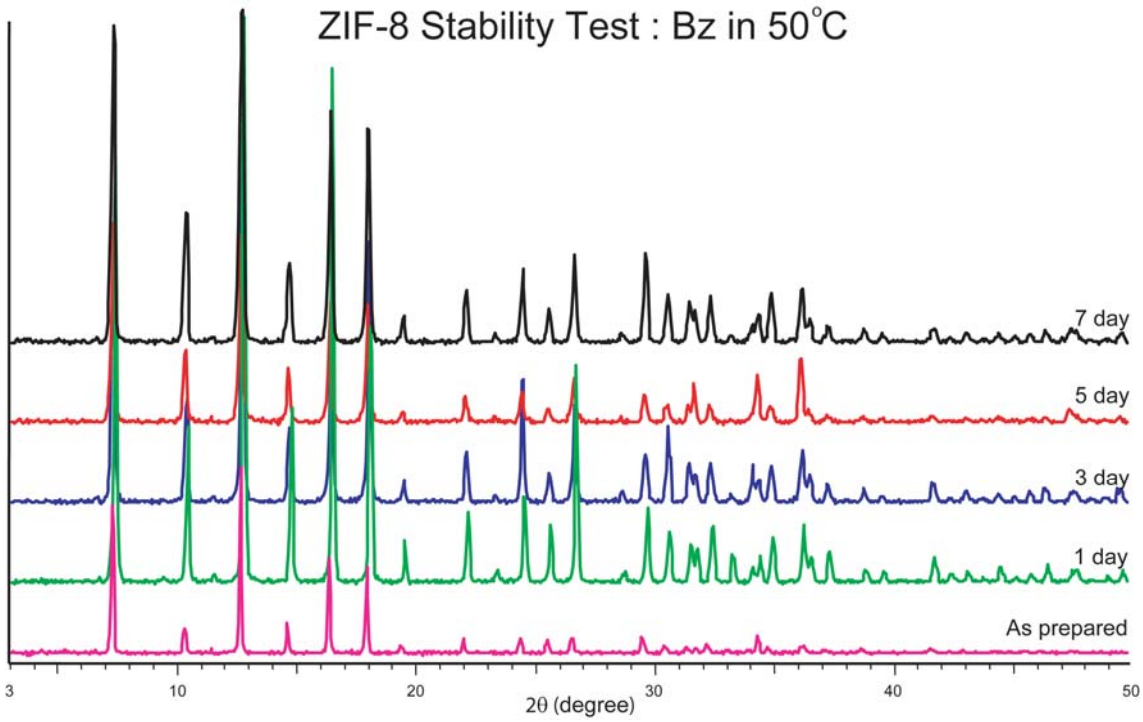

Figure S30. PXRD patterns of ZIF-8 collected during stability test in refluxing benzene. The framework structure of ZIF-8 was unchanged after 7 days.

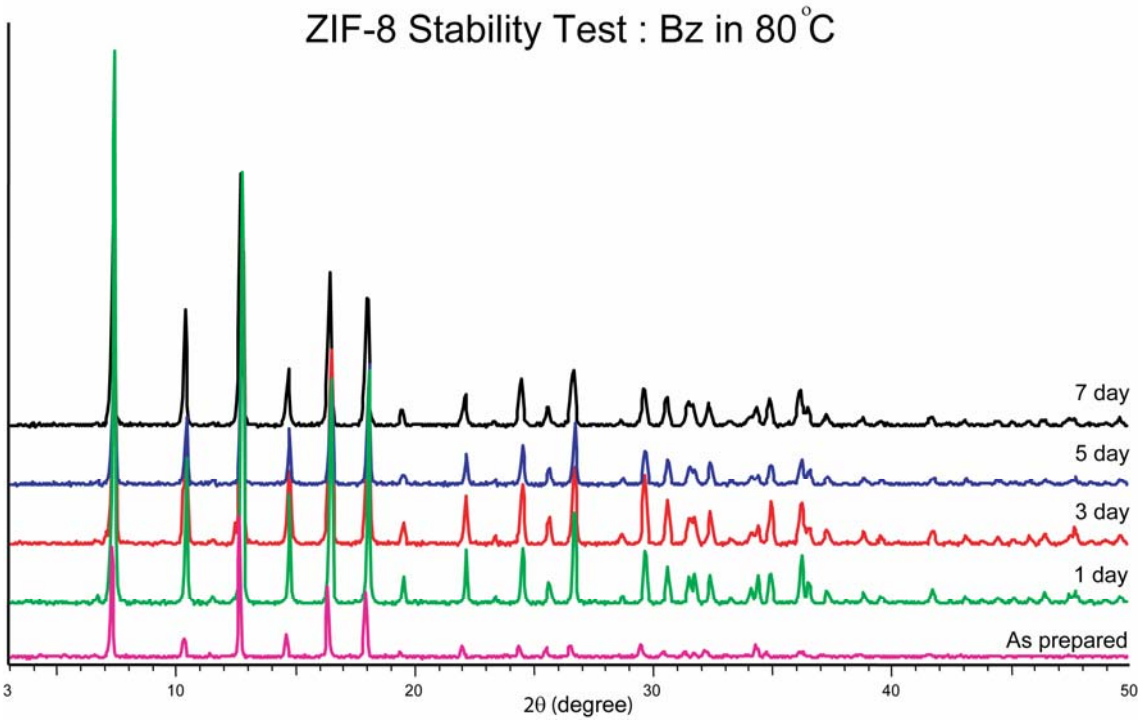

Figure S31. PXRD patterns of ZIF-8 collected during stability test in methanol at room temperature. The framework structure of ZIF-8 was unchanged after 7 days.

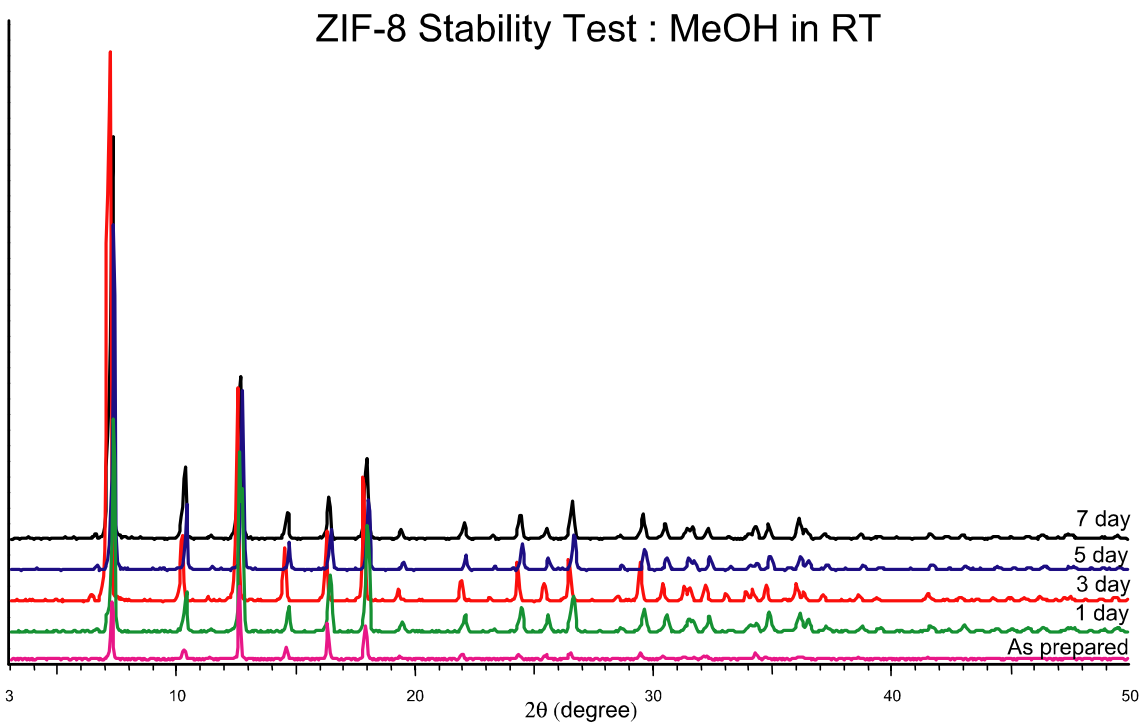

Figure S32. PXRD patterns of ZIF-8 collected during stability test in methanol at 50°C. The framework structure of ZIF-8 was unchanged after 7 days.

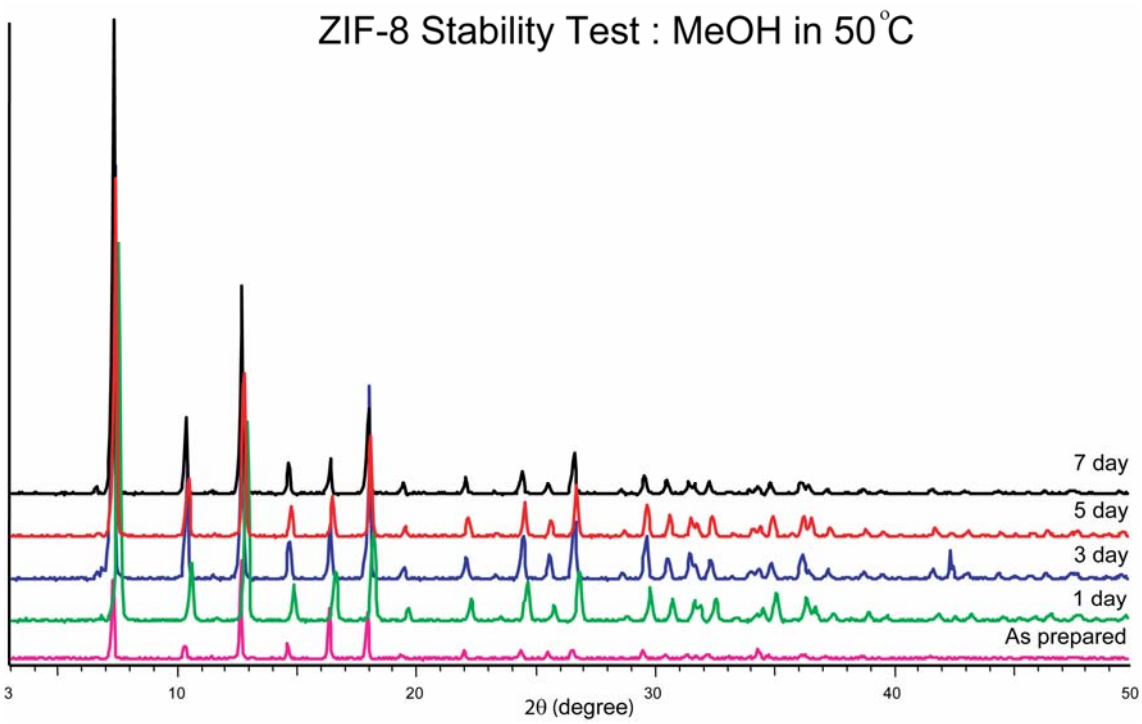

Figure S33. PXRD patterns of ZIF-8 collected during stability test in refluxing methanol. The framework structure of ZIF-8 was unchanged after 7 days.

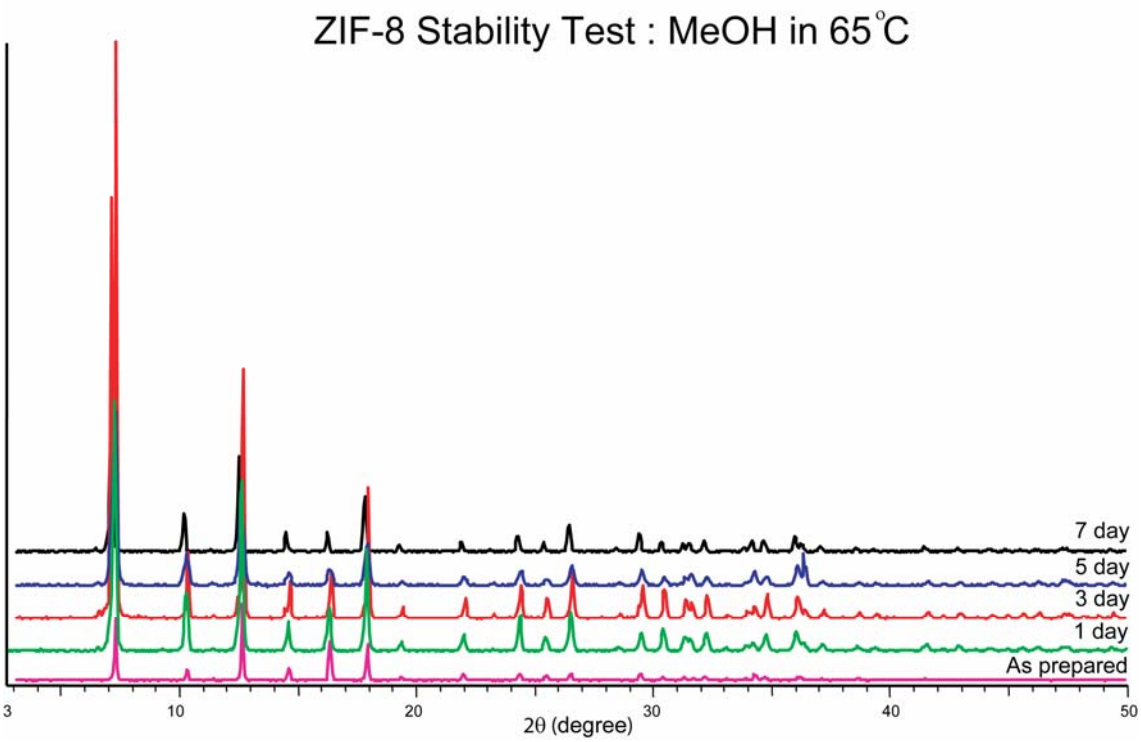

Figure S34. PXRD patterns of ZIF-8 collected during stability test in water at room temperature. The framework structure of ZIF-8 was unchanged after 7 days.

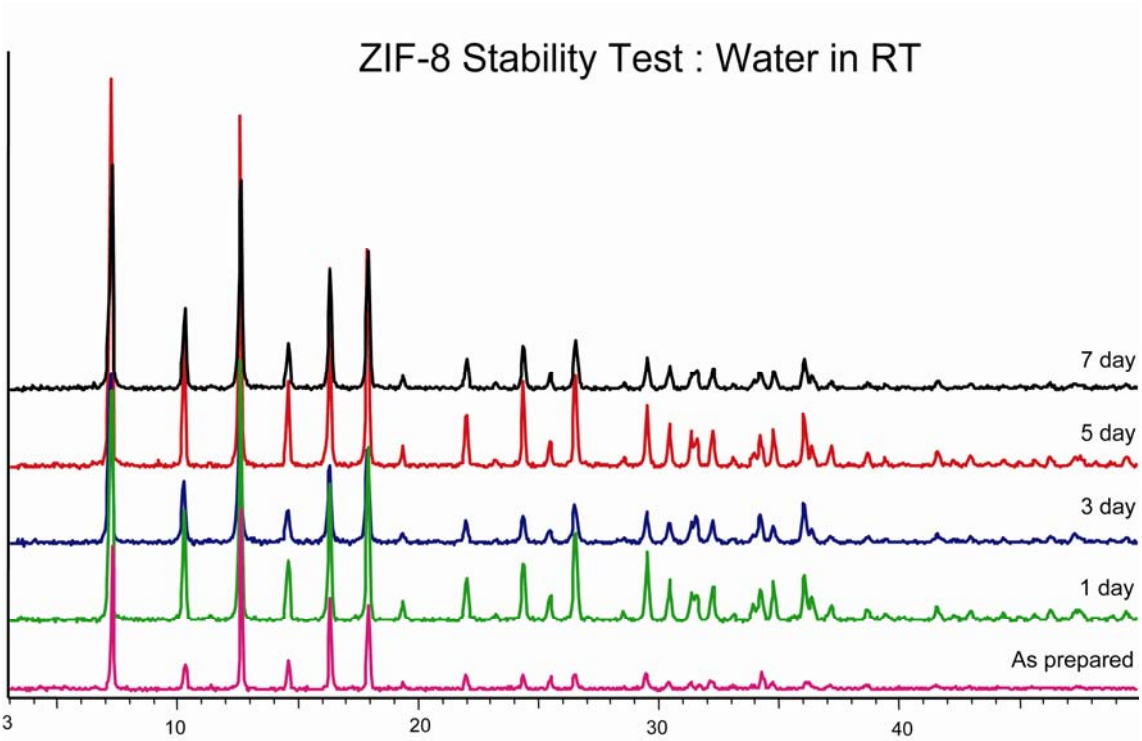

Figure S35. PXRD patterns of ZIF-8 collected during stability test in water at 50°C. The framework structure of ZIF-8 was unchanged after 7 days.

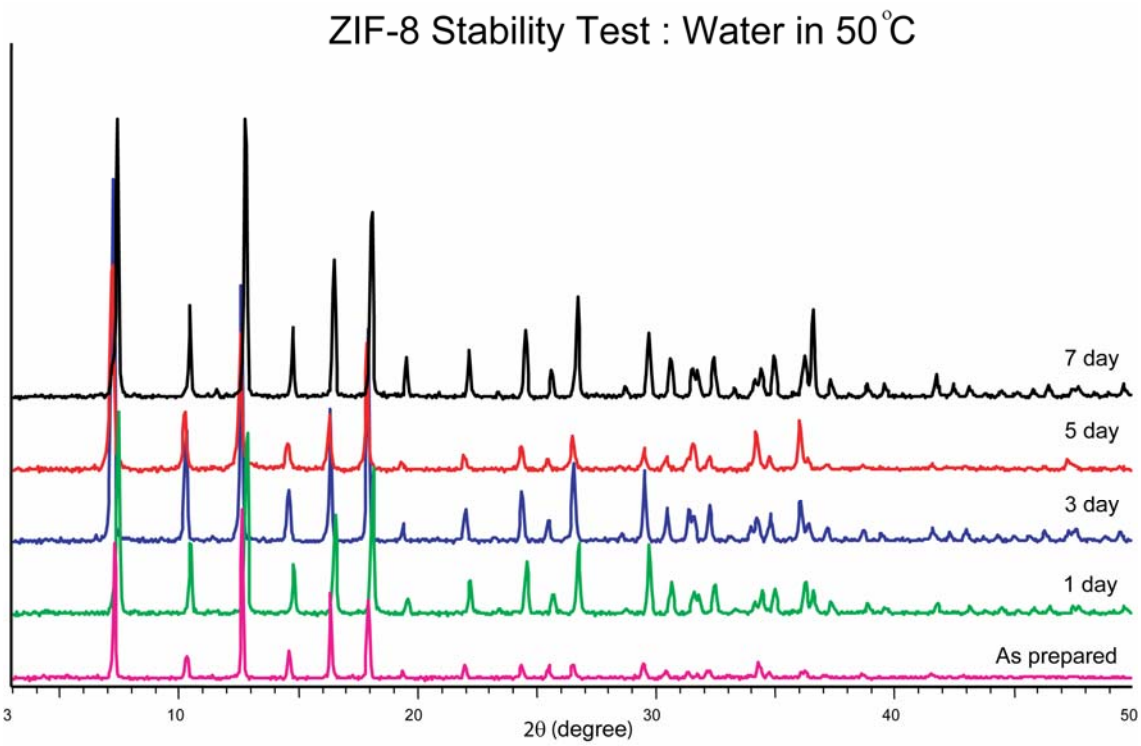

Figure S36. PXRD patterns of ZIF-8 collected during stability test in refluxing water. The framework structure of ZIF-8 was unchanged after 7 days.

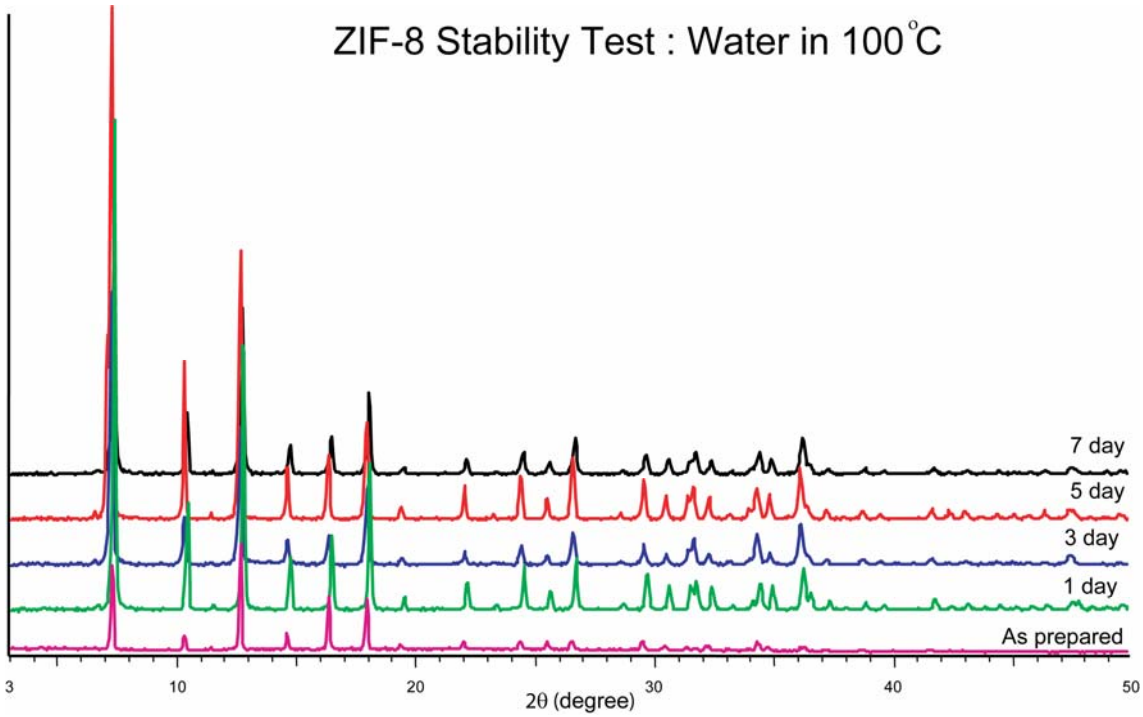

Figure S37. PXRD patterns of ZIF-11 collected during stability test in benzene at room temperature. The framework structure of ZIF-11 was unchanged after 7 days.

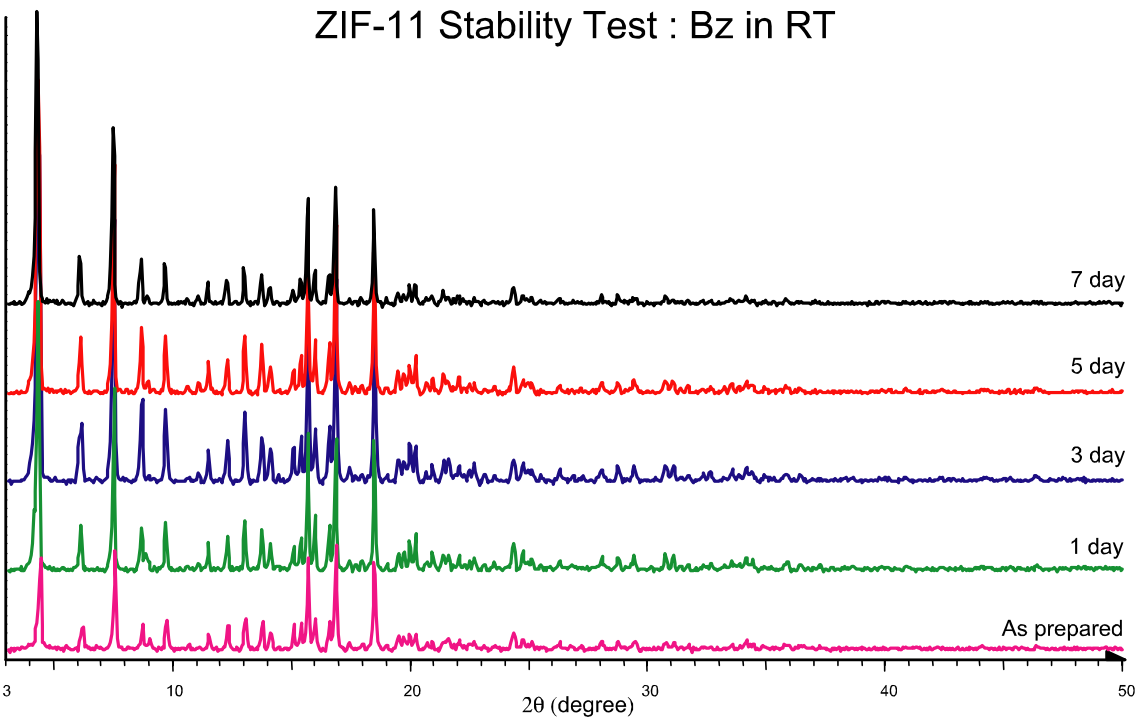

Figure S38. PXRD patterns of ZIF-11 collected during stability test in benzene at 50°C. The framework structure of ZIF-11 was unchanged after 7 days.

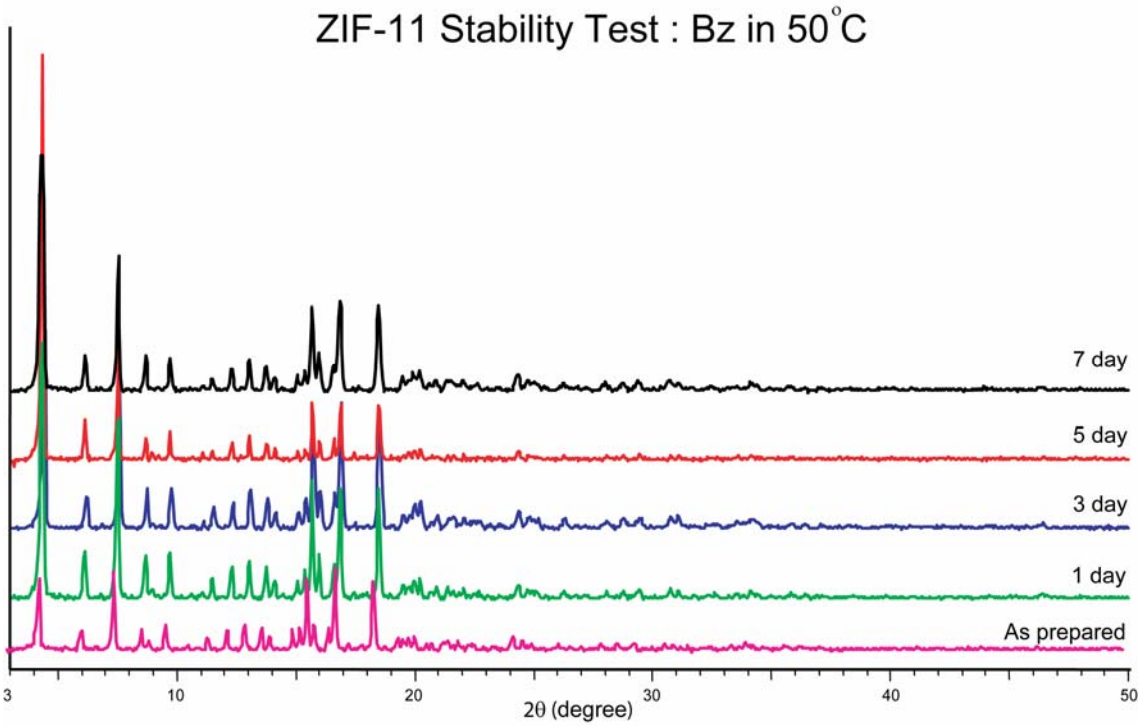

Figure S39. PXRD patterns of ZIF-11 collected during stability test in refluxing benzene. The framework structure of ZIF-11 was unchanged after 7 days.

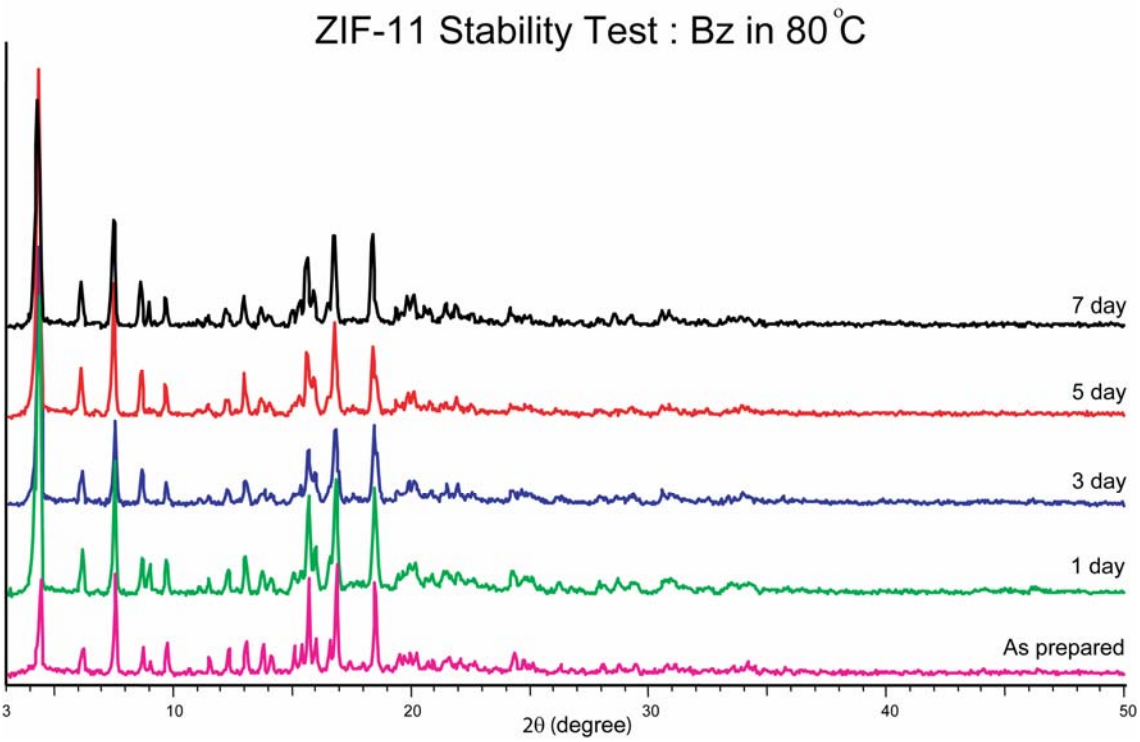

Figure S40. PXRD patterns of ZIF-11 collected during stability test in methanol at room temperature. The framework structure of ZIF-11 was unchanged after 7 days.

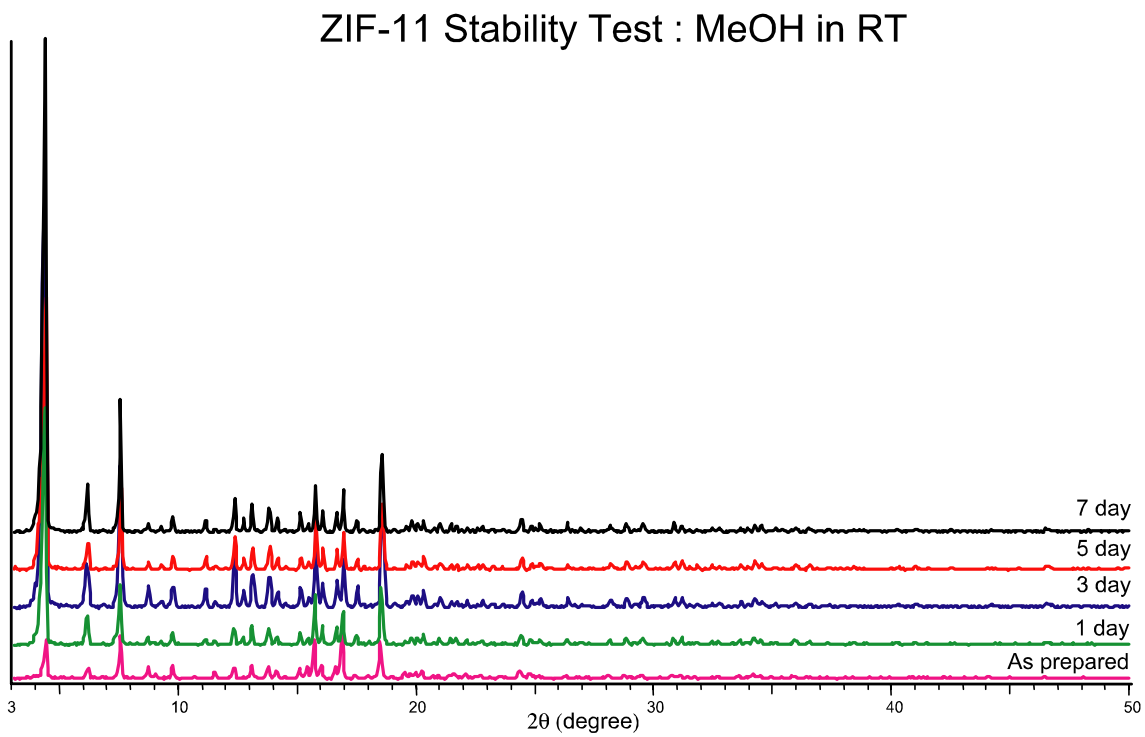

Figure S41. PXRD patterns of ZIF-11 collected during stability test in methanol at 50°C. The framework structure of ZIF-11 was unchanged after 7 days.

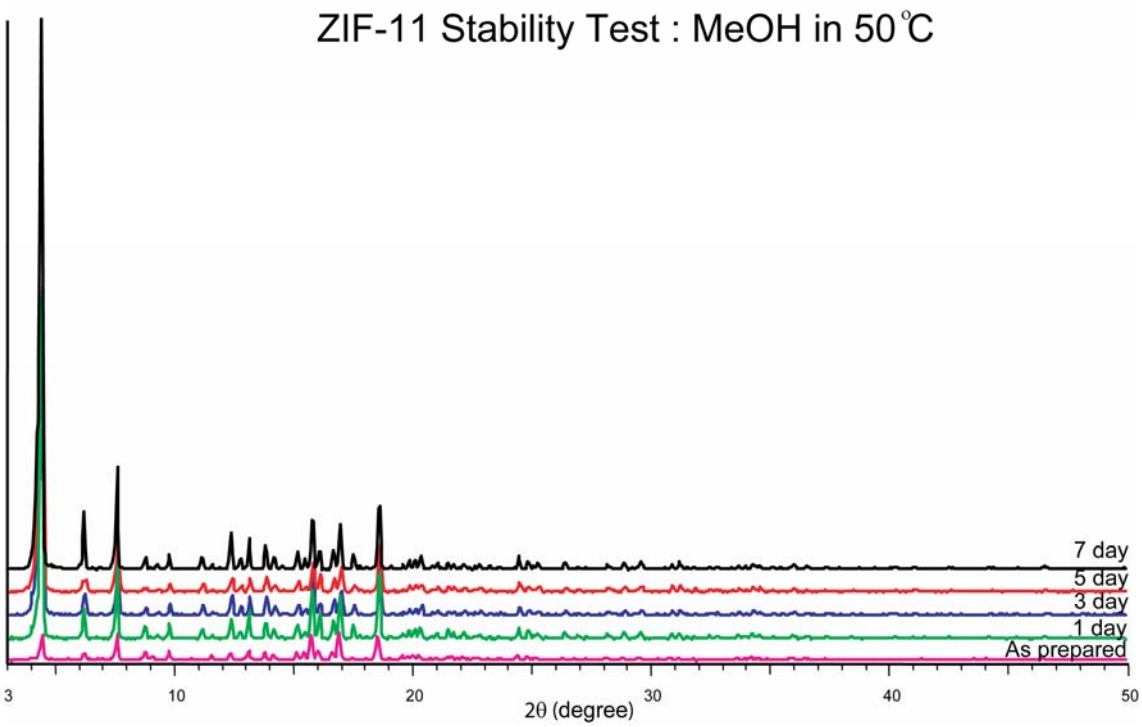

Figure S42. PXRD patterns of ZIF-11 collected during stability test in refluxing methanol. The framework structure of ZIF-11 was unchanged after 7 days.

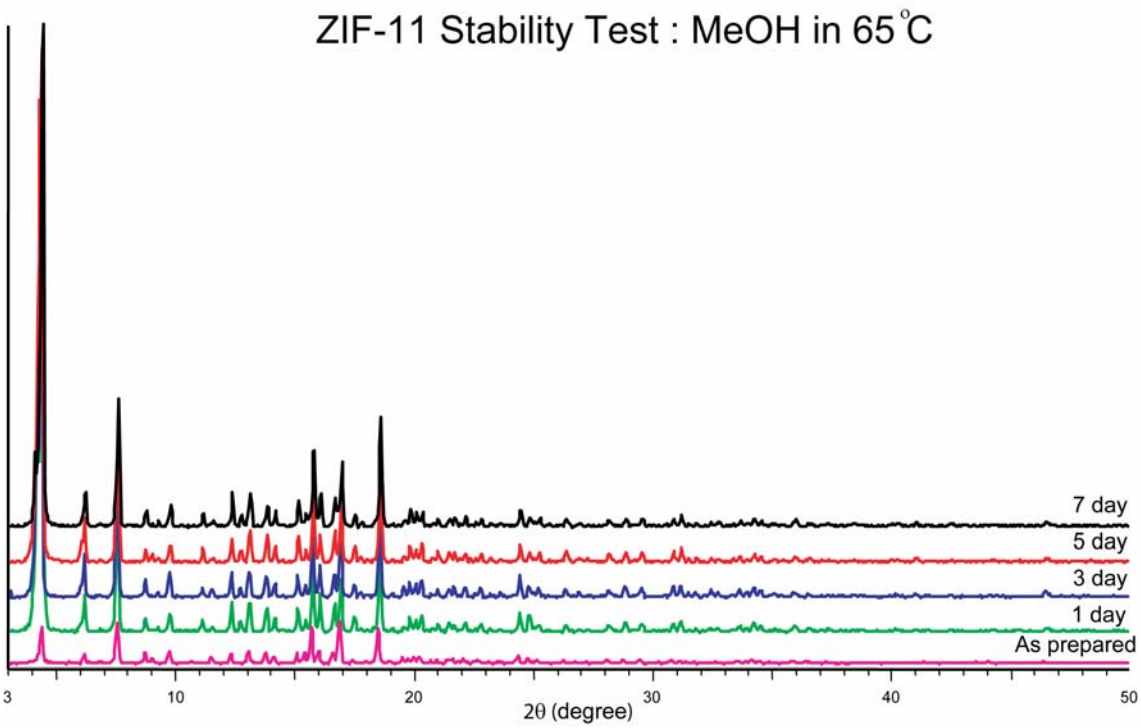

Figure S43. PXRD patterns of ZIF-11 collected during stability test in water at room temperature. The framework structure of ZIF-11 was unchanged after 7 days.

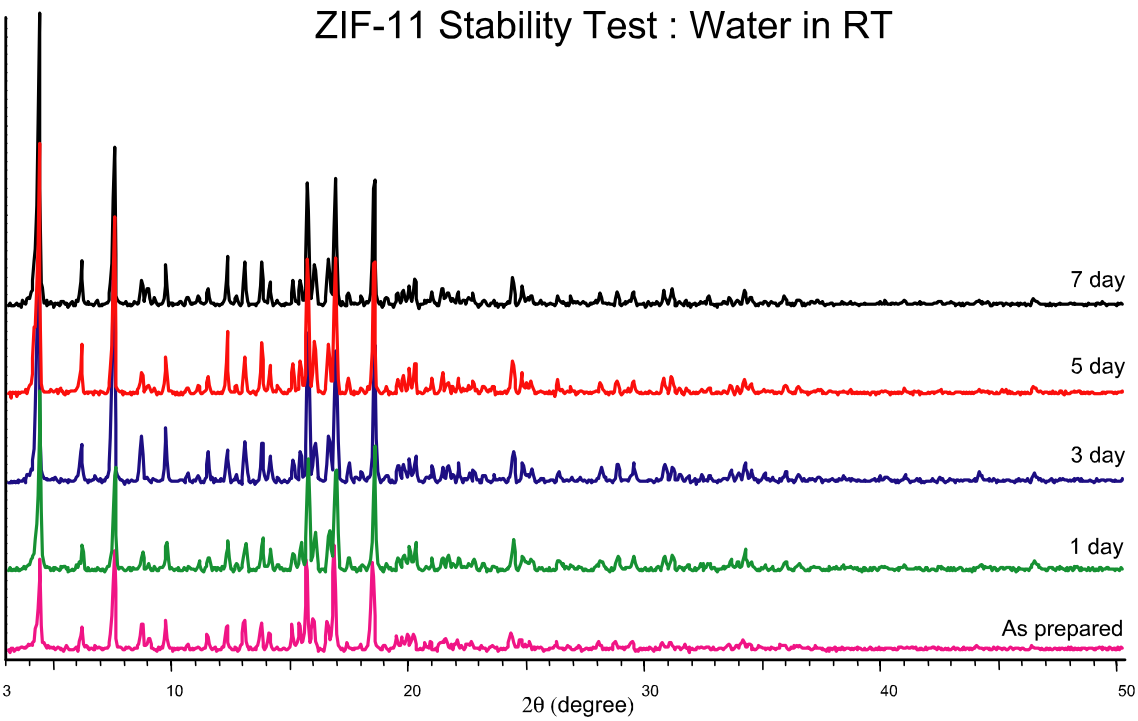

Figure S44. PXRD patterns of ZIF-11 collected during stability test in water at 50°C. The framework structure of ZIF-11 was unchanged after 7 days.

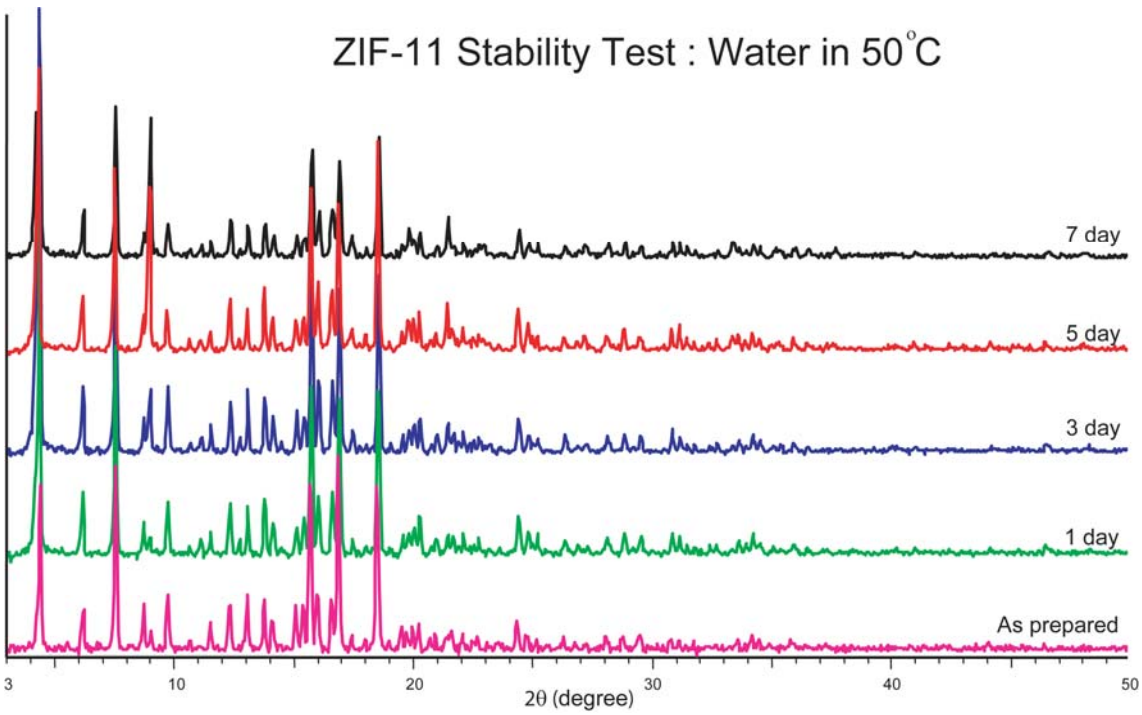

Figure S45. PXRD patterns of ZIF-11 collected during stability test in refluxing water. ZIF-11 transformed to another crystalline material after 3 days.

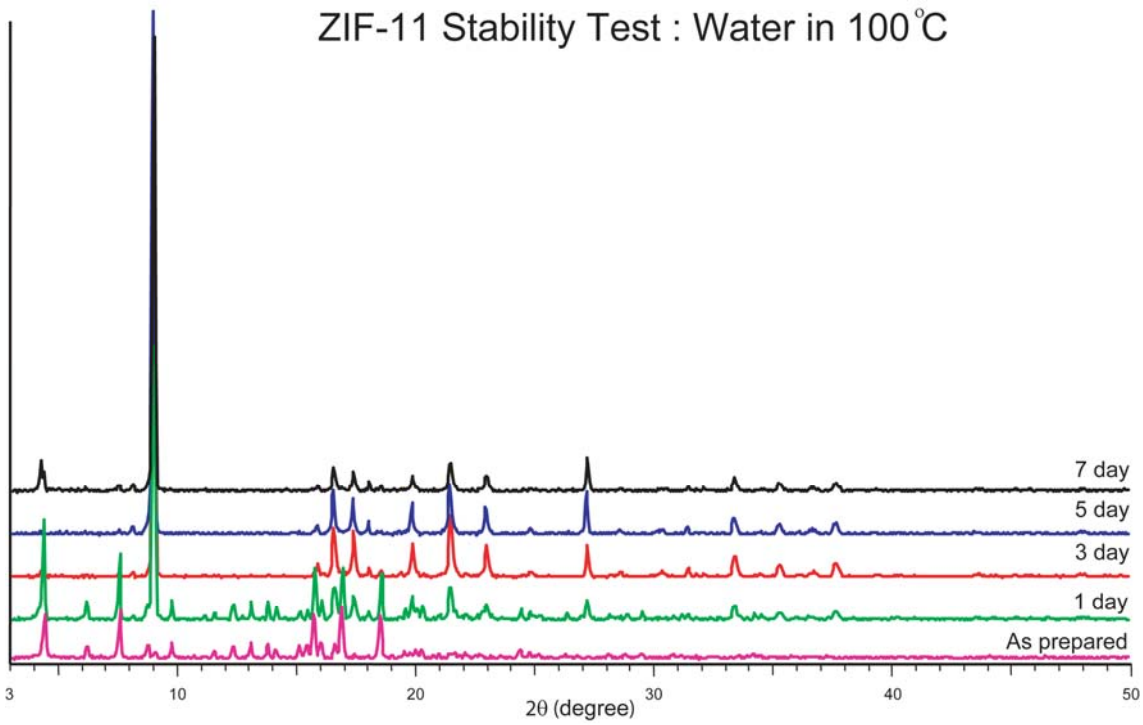

Section 5. TGA, Guest Mobility and Thermal Stability

All samples were run on a TA Instruments Q-500 series thermal gravimetric analyzer with samples held in platinum pans in a continuous flow nitrogen atmosphere. Samples were heated at a constant rate of 5 °C/min during all TGA experiments.

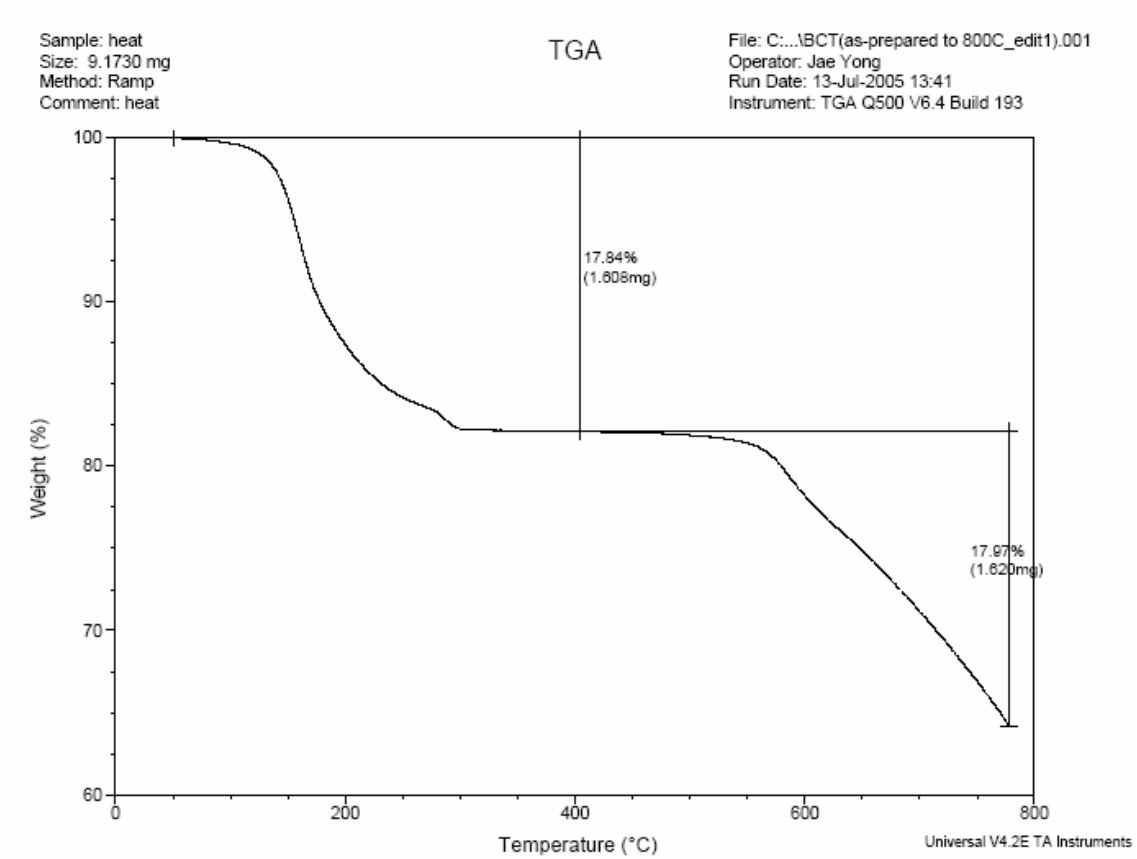

Figure S46. TGA trace of as-synthesized ZIF-1 (**crb**)

The first weight-loss step of 17.8 % corresponds to the loss of all guest molecules (1 Me_2NH; Calcd. 18.4 %). The second weight-loss step corresponds to the decomposition of framework.

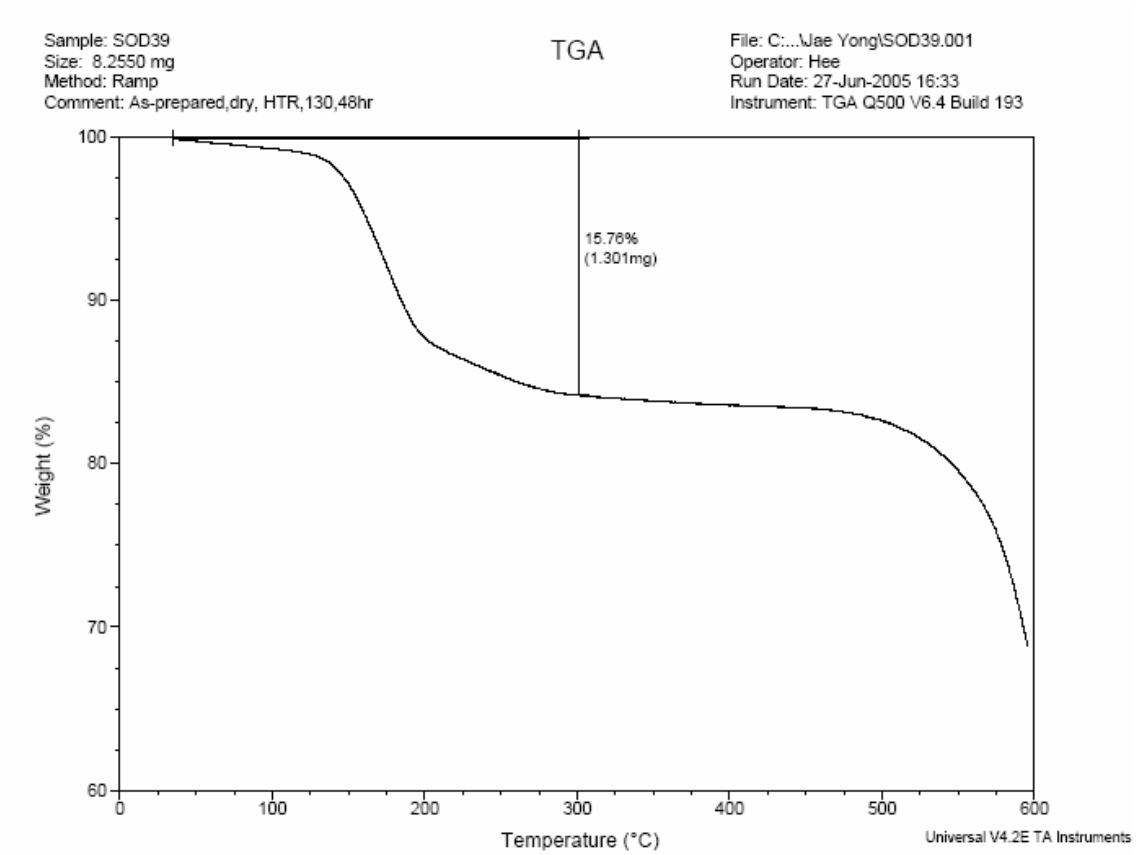

Figure S47. TGA trace of as-synthesized ZIF-7 (**sod**).

The first weight-loss step of 15.8% corresponds to the loss of all guest molecules (3 H_2O; Calcd. 15.2 %). The second weight-loss step corresponds to the decomposition of framework.

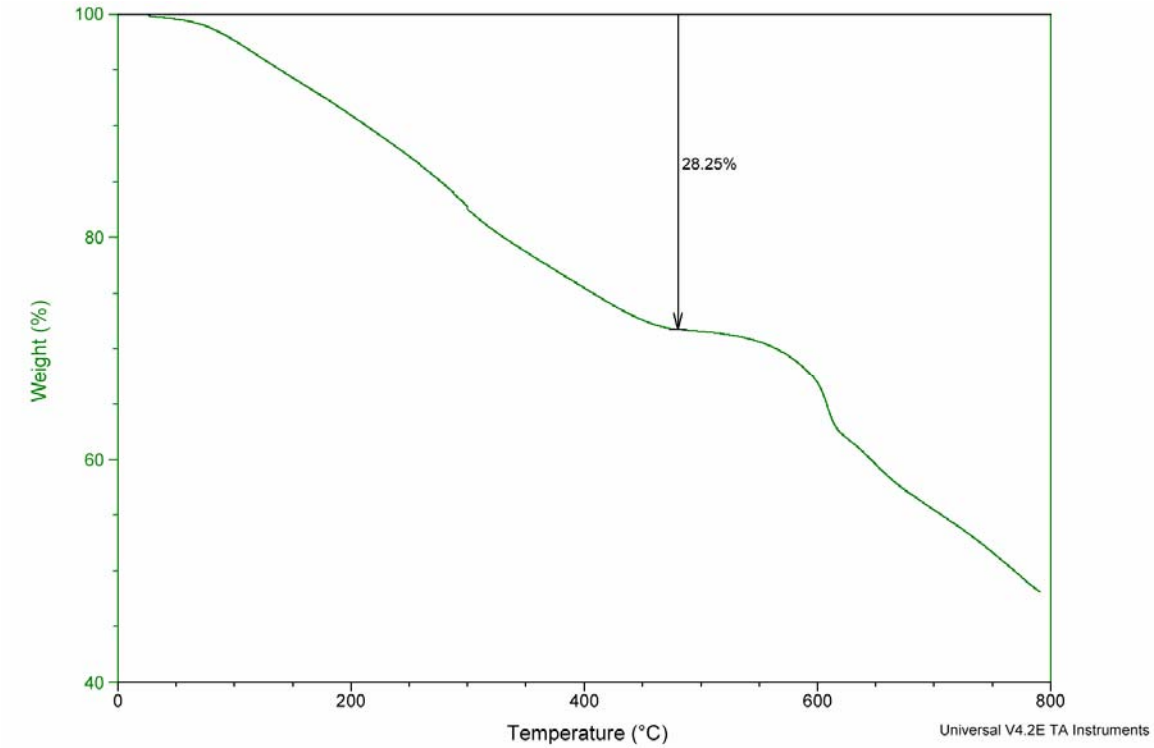

Figure S48. TGA trace of as-synthesized ZIF-8 (**sod**).

The weight-loss step of 28.3% (ambient temperature to 450 °C) does not correspond to the escape of all guest molecules in as-synthesized ZIF-8 (1 DMF and 3 H_2O; calcd. 35.9%). Since the guest molecules are expected to leave the restricted porous system slowly, we interpret this deviation as arising from the carbonization of guests in the pores at high temperature. This view is supported by our observation that the color of an as-synthesized ZIF-8 sample turns dark after it has been heated to 500 °C in nitrogen atmosphere and held at this temperature for 1 hour, however, its crystal morphology is well-maintained and the PXRD pattern of such a sample matches the one simulated from the single crystal structure of ZIF-8.

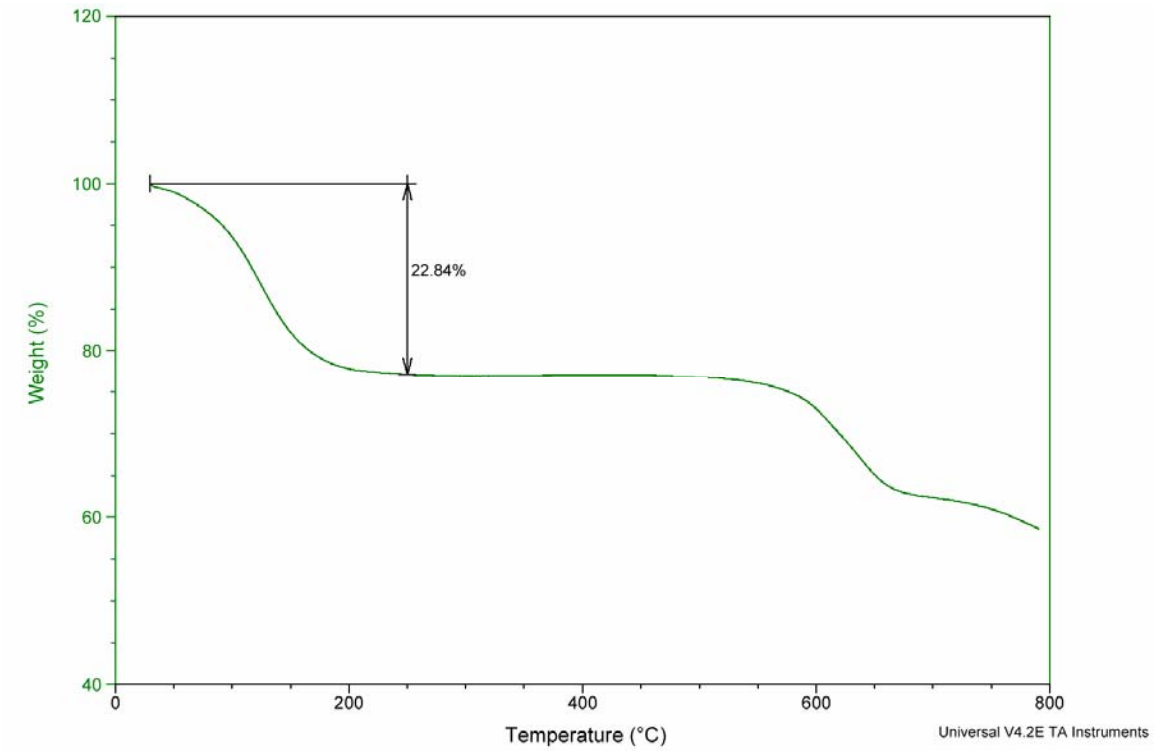

Figure S49. TGA trace of as-synthesized ZIF-11 (**rho**).

The first weight-loss step of 22.8% (ambient temperature to 250 °C) corresponds to the escape of all DEF solvent molecules trapped in the pores (0.9 DEF; calcd. 23.3%), despite the fact that DEF is actually much larger than the aperture of ZIF-11 in size. The TGA result combined with the PXRD evidence shown below have led us to view ZIF-11 as a dynamic structure at elevated temperatures such that the orientation of imidazolate type links can be adjusted reversibly to allow guest species to escape without sacrificing the integrity of the framework.

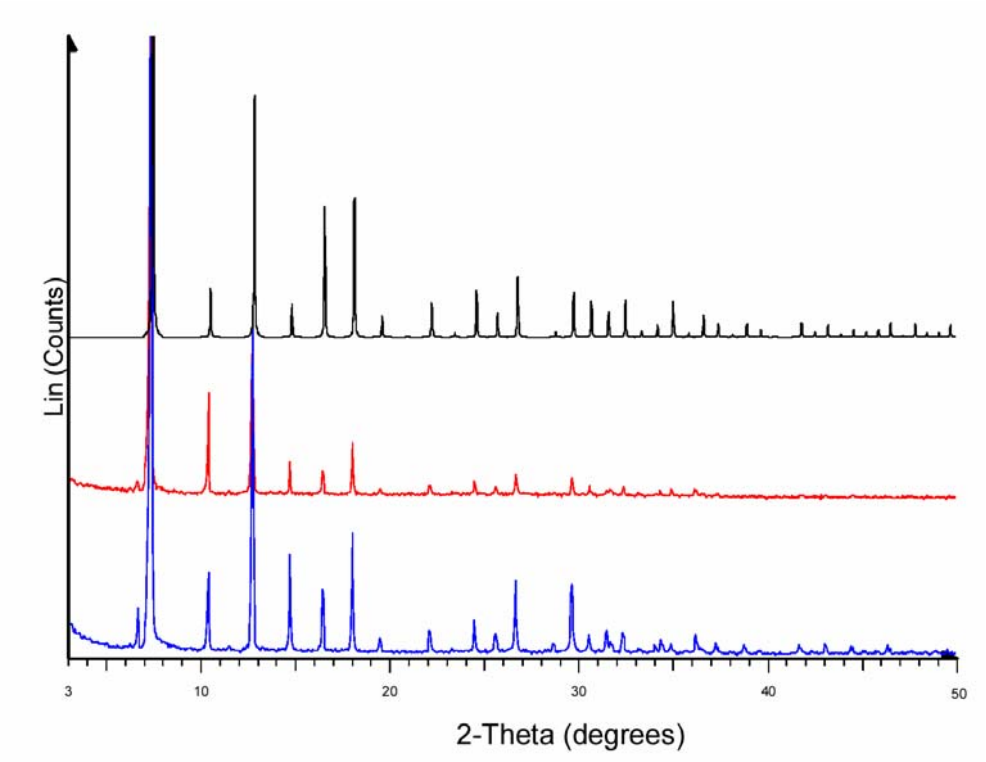
Lin (Counts)
3
10
20
30
40
50
2-Theta (degrees)

(a)

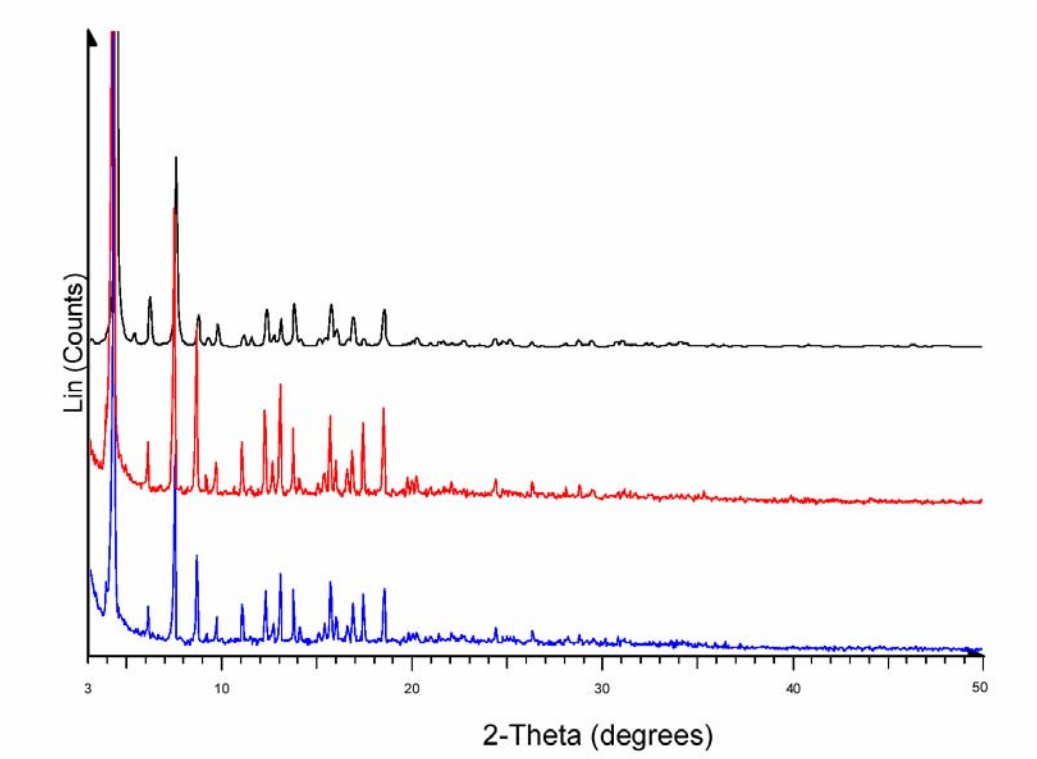
Lin (Counts)
3
10
20
30
40
50
2-Theta (degrees)

(b)

Figure S50. The PXRD patterns of (a) ZIF-8: as-synthesized sample in black, as-synthesized sample after being heated to 500 °C in N_2 and held for 1 hour in red, evacuated sample in blue; (b) ZIF-11: as-synthesized sample in black, as-synthesized sample after being heated to 300 °C in N_2 and held for 1 hour in red, evacuated sample in blue.

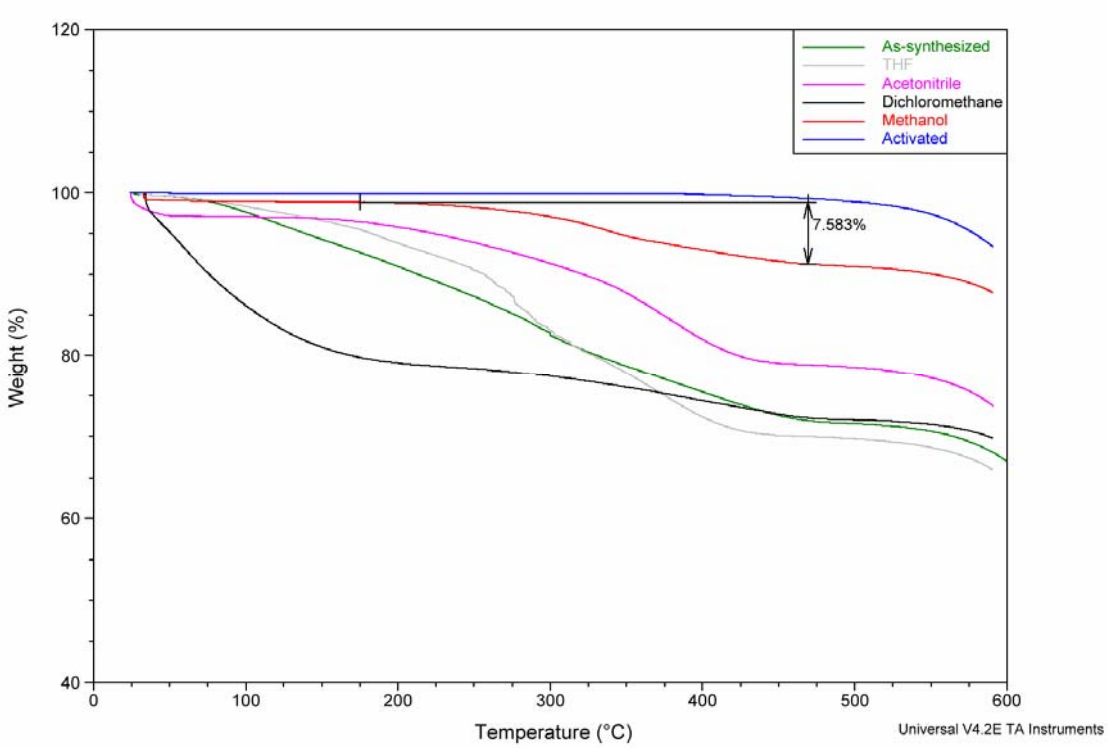
As-synthesized
THF
Acetonitrile
Dichloromethane
Methanol
Activated
7.583%
Weight (%)
Temperature (°C)
Universal V4.2E TA Instruments

(a)

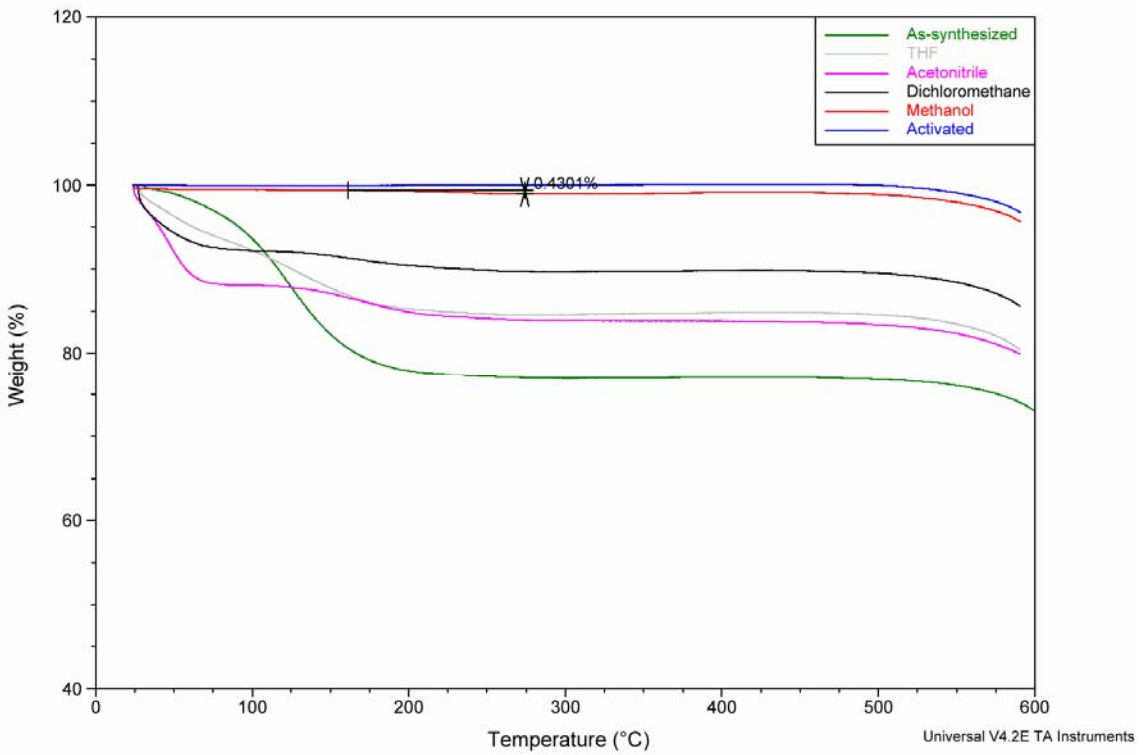
As-synthesized
THF
Acetonitrile
Dichloromethane
Methanol
Activated
0.4301%
Weight (%)
Temperature (°C)
Universal V4.2E TA Instruments

(b)

Figure S51. The overlay of TGA traces of as-synthesized, solvent-exchanged, and evacuated (activated) samples of (a) ZIF-8 and (b) ZIF-11.

The TGA traces of ZIF-8 samples after being immersed in various solvents at ambient temperature were shown in Figure S51a. Clearly, treatment with methanol or dichloromethane simplified the thermogravimetric behavior of ZIF-8 significantly, indicative of effective solvent-exchange. In particular, in the TGA trace of methanol-exchanged ZIF-8 sample, the original gradual weight-loss step of 28.3% up to 450 °C were replaced by a very small initial step at near-ambient temperature, a plateau up to 200 °C and a gradual step of 7.6% in the temperature range 200 - 450 °C. As shown in Figure S51b, ZIF-11 could be much more effectively solvent-exchanged, most clearly in the case of methanol-exchanged sample whose TGA trace only showed a tiny weight-loss step of 0.4% in the temperature range 150 - 250 °C. Once again, ZIF-11 appears to be a more dynamic structure than ZIF-8.

Section 6. Gas-Sorption Analyses

All low-pressure gas-sorption experiments (up to 1 atm) were performed on a Quantachrome Autosorb-1C automatic volumetric instrument. High-pressure hydrogen sorption experiments (up to 80 bar) were performed on a VTI HPA-100 volumetric instrument equipped with a home-made liquid nitrogen cooling system to sustain a constant coolant bath level. The compressibility factors of high-pressure gases were determined by using the NIST RefProp program (version 7.0) and the NIST Standard Reference Data Base 23 (for details of high-pressure hydrogen sorption measurements, see Wong-Foy, A. G., Matzger, A. J. & Yaghi, O. M. (2006) *J. Am. Chem. Soc.* **128**, 3494-3495).

In light of the TGA results shown in the previous section, ZIF-8 and ZIF-11 were evacuated in the following way prior to gas-sorption analysis. The as-synthesized ZIF samples were immersed in methanol at ambient temperature for 48 h, evacuated at ambient temperature for 5 h, then at an elevated temperature (300 °C for ZIF-8, 180 °C for ZIF-11) for 2 h. ZIF samples thus obtained were optimally evacuated, as evidenced by their well-maintained PXRD patterns and the long plateau (ambient temperature to 550 °C) in their TGA traces, shown in Figures S50 and S51.

In addition to the gas sorption isotherms shown in the main text, more detailed analysis of ZIF-8 were performed, and the results were shown below.

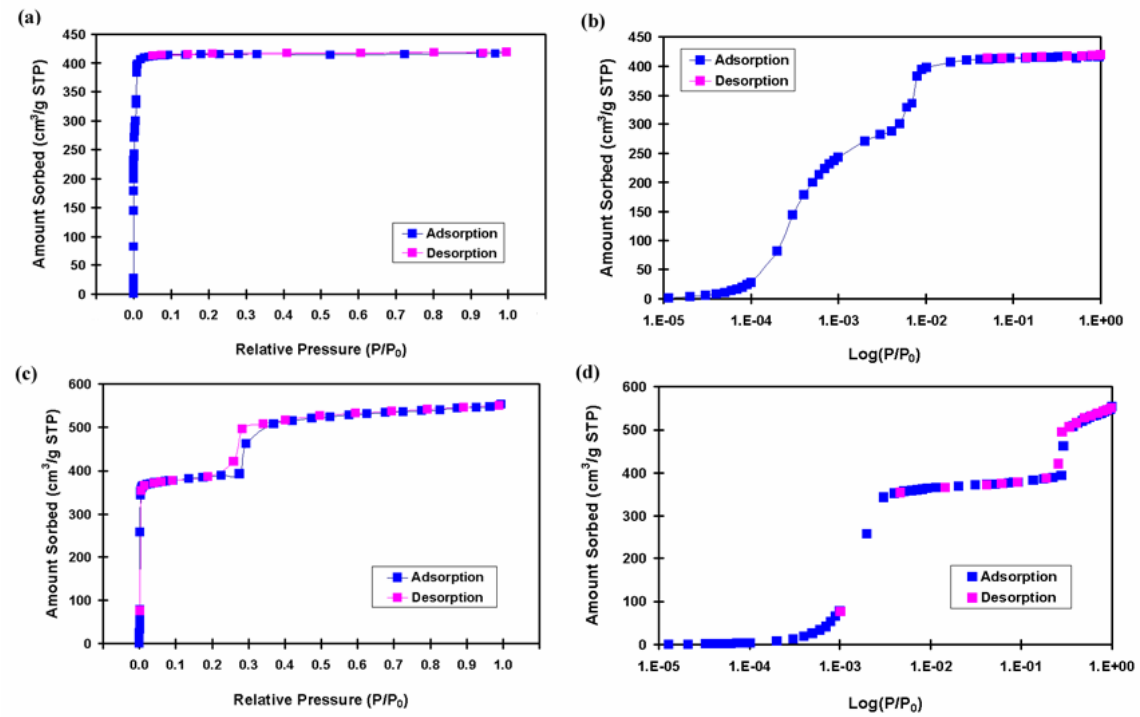

Figure S52. Gas sorption isotherms for ZIF-8 (**sod**): (a) linear-scale plot and (b) logarithmic-scale plot of N_2 sorption isotherm at 77K; (c) linear-scale plot and (d) logarithmic-scale plot of Ar sorption isotherm at 87K.

The microporous nature of evacuated ZIF-8 was unequivocally proven by this compound's Type I nitrogen sorption isotherm, as shown in Figure S52a. In the logarithmic-scale plot of the same isotherm, shown in Figure S52b, two consecutive N_2 uptake steps in the micropore region were revealed, occurring at $P/P_0 = 1\times10^{-4}$ - 2×10^{-3} and 5×10^{-3} - 1×10^{-2}, respectively. The two-step feature was found in the argon sorption isotherm at 87 K for ZIF-8 as well, shown in Figure S52c-d. Interestingly, the two steps in the argon isotherm were much more separated, occurring at $P/P_0 = 1\times10^{-3}$ - 3×10^{-3} and 0.25 - 0.35, respectively. With the latter step being a quite steep hysteresis loop, this

argon isotherm should be classified as a typical Type IV. However, the hysteresis loop cannot be explained by capillary condensation of argon into mesopores because of its low closure point, and more importantly, because of the lack of any step and hysteresis feature in the mesopore range of the nitrogen isotherm for ZIF-8. Neither is it plausible to attribute the two-step features to a change in the structure of ZIF-8 that allows further accommodation of significant amount of gas molecules because such effect was not observed in ZIF-11, which has been shown previously to be a more dynamic structure than ZIF-8 at elevated temperatures or in solvents. Therefore, we interpret the two-step features in both nitrogen and argon isotherms as a result of a reorganization of the adsorbed gas molecules occurred at a certain threshold pressure, and this effect is very significant in the case of ZIF-8 because its aperture size is very close to the sizes of nitrogen and argon molecules. Further, we speculate that the large difference between the threshold pressures for the second steps in nitrogen and argon isotherms is due to the different polarizabilities and molecular shapes of nitrogen and argon, which in turn determine how the adsorbed gas molecules distribute and reorganize after the completion of the first steps.

Apparent surface areas of 1,810 m^2/g (Langmuir) and 1,630 m^2/g (BET) for ZIF-8 were obtained by using the data points on the adsorption branch in the range of P/P_0 =

0.01 - 0.10, and a micropore volume of 0.636 cm^3/g for ZIF-8 was obtained based on a single data point at P/P_0 = 0.10. The linearity of fitting to Langmuir equation is 1.000000, to BET equation is 0.999710, and the C constant derived from BET equation is –663. Therefore, Langmuir model appears to be more suitable for evaluating the surface area of ZIF-8.

Using the data points on the nitrogen isotherm in the range of $P/P_0 = 7\times10^{-4}$ - 4×10^{-3}, i.e. at the completion of the first step, a Langmuir surface area of 1334 m^2/g (linearity 0.999997), a BET surface area of 1328 m^2/g (linearity 0.999998, C constant 3900), and a micropore volume of 0.443 cm^3/g (at $P/P_0 = 4\times10^{-3}$) were obtained. Using the data points on the argon isotherm in the range of $P/P_0 = 5\times10^{-3}$ - 5×10^{-2}, i.e. at the completion of the first step, a Langmuir surface area of 1430 m^2/g (linearity 0.999996), a BET surface area of 1353 m^2/g (linearity 0.999961, C constant –7890), and a micropore volume of 0.481 (at P/P_0 = 0.10) were obtained. The values derived from nitrogen isotherm and argon isotherm match well. Using a single data point on the adsorption branch of argon isotherm at P/P_0 = 0.42, i.e. at the completion of the second step, a micropore volume of 0.656 cm^3/g was obtained. Again, the value matches the one derived from the counterparts in the nitrogen isotherm. These calculations show the similarity between the two-step features in nitrogen and argon isotherms. However, for

the purpose of reporting surface area and micropore volume, we have adopted the method as described in the previous paragraph (also in the main text of the manuscript) because the values thus derived can be more readily compared with the ones reported in literature.

Interestingly, very similar "sub-steps" and hysteresis loop in the region P/P_0 = 0.12-0.15 have been know for a long time in the Ar (77 K) and N_2 (77 K) isotherms for zeolite ZSM-5, especially in its hydrophobic pure silica form, i.e. Silicalite-1. Please see Rouquerol, F., Rouquerol, J & Sing, K. (1999) in *Adsorption by Powders & Porous Solids: Principles, Methodology and Applications* (Academic Press, London), pp. 389-396 or the original literatures:

Muller, U. & Unger, K. K. (1988) in *Characterization of Porous Solids I*, eds. Unger, K. K., Rouquerol, J., Sing, K. S. W. & Kral, H. (Elsevier, Amsterdam), pp. 535

Muller, U., Reichert, H., Robens, E., Unger, K. K., Grillet, Y., Rouquerol, F., Rouquerol, J., Pan, D. & Mersmann, A. (1989) Fresenius Z. Anal. Chem.

Llewellyn, P. L., Coulomb, J.-P., Grillet, Y., Patarin, J., Lauter, H., Reichert, H. & Rouquerol, J. (1993) *Langmuir* **9**, 1846

Llewellyn, P. L., Coulomb, J.-P., Grillet, Y., Patarin, J., Andre, G. & Rouquerol, J. (1993) *Langmuir* **9**, 1852

The aforementioned sub-steps and hysteresis loop in the pre-condensation region were attributed to phase transitions of the adsorbates confined within the pores of ZSM-

5 based on the evidence of microcalorimetry and neutron diffraction. Therefore, it is entirely reasonable for us to interpret the steps and hysteresis loops we observed in ZIF-8 system as reorganization of adsorbates occurred at certain threshold pressures. A thorough investigation of these step features of the isotherms for ZIF-8 is underway and the results will be summarized for a publication in the near future.